Reviews

of Geophysics and Space Physics ©

VOLUME 8 FEBRUARY 1970 NUMBER 1

Physical Mechanisms of Seismic-Wave Attenuation[1]

DAVID D. JACKSON[2]

Department of Geology and Geophysics
Massachusetts Institute of Technology
Cambridge, Massachusetts 02139

DON L. ANDERSON

California Institute of Technology
Seismological Laboratory
Pasadena, California 91109

Abstract. The theoretical and experimental evidence concerning mechanisms likely to be responsible for the attenuation of seismic waves are reviewed. Intergranular thermoelastic relaxation, atomic diffusion, and dislocation mechanisms cannot be ruled out as significant causes of seismic attenuation, but the most effective mechanisms seem to be associated with partial melting, grain-boundary relaxation, and a poorly understood mechanism called 'high-temperature, internal-friction background' which obeys an equation of the form

$$Q^{-1} = (A/f) \exp(-H^*/RT)$$

Here Q^{-1} is a dimensionless measure of anelasticity, f is the frequency, T is the absolute temperature, and A, H^*, and R are constants for a material of uniform composition and grain size. Many of the mechanisms considered here have a strongly frequency-dependent Q^{-1}. However, in a material as complex as a rock, there is unlikely to be a single discrete relaxation time or activation energy, or a single 'typical' grain size. The ob-

[1] Contribution 1570, Division of Geological Sciences, California Institute of Technology, Pasadena.

[2] Now at Institute of Geophysics and Planetary Physics, University of California, Los Angeles, California 90024.

served Q^{-1} is likely to result from a superposition of several mechanisms and involve a spectrum of parameters leading to weaker frequency dependence than is predicted from a single simple mechanism. The seismic data cannot at present resolve the question of whether or not Q^{-1} has an intrinsic frequency dependence. The extent and the limitations of the available seismic data are discussed. Experimental data on the attenuation of oxides are summarized, the measurements at high temperature and low frequency being emphasized.

The elastic properties of a solid are controlled mainly by the interatomic forces of the crystalline lattice and to a good approximation are functions of the molar volume alone. The intrinsic effect of temperature at constant volume is small and, in general, temperature can be treated as a small perturbation. Elastic properties therefore supply information about composition and density; pressure, temperature, solid-solution effects, and polymorphism affect these properties through their effect on the density. The seismic velocities in the earth have yielded estimates of the composition and density in the various regions.

Anelastic properties of solids are controlled by the thermal and defect properties. Depending on the mechanism, these properties are influenced by thermal conductivity, grain size, defect concentration and mobility, diffusion rate, and on the relatively weak interatomic and interdefect bonds at grain boundaries. Many of the mechanisms are activated processes that depend very strongly on temperature and, to a small extent, pressure.

Recent advances in seismology have made it possible to measure the attenuation of seismic body and surface waves at different frequencies. Properly interpreted, these measurements may reveal the 'anelastic' properties of the earth as a function of depth. It is important for solid-earth geophysicists to interpret the attenuation of seismic waves properly and derive as much information as possible from these measurements, since they complement the measurements of elastic properties. Although laboratory work on rocks and minerals of geophysical interest has lagged behind the seismic work, laboratory data on other materials, combined with existing theories of anelasticity, provide a useful framework for interpreting the new seismic data.

There are several commonly used measures of attenuation (see, for example, *Gellings* [1961]). In this discussion we shall use 'internal friction,' Q^{-1}, defined by $Q^{-1} = (1/2\pi)\ \Delta W/W$, where W is the total amount of elastic energy stored per unit volume per cycle, and ΔW is the part of W that is dissipated per cycle. The parameter Q is often called the 'quality factor.' For linear mechanisms (i.e., those such that a sinusoidal stress input gives an output of the same frequency, and such that Q^{-1} is independent of the strain amplitude) we have $Q^{-1} = \tan \delta$, where δ is the phase lag between stress and strain. Otherwise, detailed consideration of the energy loss is needed to compute Q^{-1}.

Most of the geophysical literature on attenuation of seismic waves is concerned with the macroscopic phenomenology of absorption. Several excellent reviews of this aspect of the subject have appeared [*Knopoff*, 1964; *Knopoff and MacDonald*, 1960; *Futterman*, 1962; *Strick*, 1967]. Undue attention has been paid to mechanisms, both linear and nonlinear, that give an internal friction

which is absolutely independent, or only very weakly dependent, on frequency, even though the presently available seismic data make no such demands. Little attention has been paid to the possible microscopic or atomistic causes of seismic-wave absorption. Although there is a vast literature on attenuation mechanisms by solid state physicists, metallurgists, and ceramicists, much of it is phenomenological, and, because of interest in low temperatures, low pressures, high frequencies, high purities, and single crystals, much of it is not relevant to seismic problems.

Knopoff [1964] reviewed the geophysics literature on attenuation, taking a phenomenological approach. He pointed out that in the earth and in rocks attenuation appears to be linear. The internal friction of rocks, as measured in the laboratory, is roughly independent of frequency from 1 to 10^6 Hz, is higher by an order of magnitude or more in polycrystals than in single crystals, and is responsible for very little dispersion, if any. Seismic experiments in sandstone, shale, and soils indicate that the internal fricton is independent of frequency from 100 to 1000 Hz. Knopoff reviews several linear and nonlinear phenomenological models that account for the frequency-independent internal friction, but devotes little discussion to the microscopic mechanisms that might be responsible for such behavior.

Observations of earthquake-induced seismic waves suggest that the attenuation of shear waves is greater than that of compressional waves. In the upper mantle of the earth the shear wave internal friction is in the range of $6–9 \times 10^{-3}$, and in the lower mantle it is of the order of 7×10^{-4}.

Gordon and Nelson [1966] have reviewed some of the possible seismic attenuation mechanisms and emphasized the importance of frequency-dependent and thermally activated processes. They rank viscous grain-boundary damping, stress-induced ordering, and dislocation damping as the most probable sources of seismic attenuation. *Anderson and Archambeau* [1964] briefly discussed thermally activated mechanisms, assuming an internal friction of the form $Q^{-1} = C \cdot \exp[-(E^* + PV^*)/RT]$, where C is a constant independent of temperature, pressure, or frequency, E^* and V^* are activation energy and activation volume, and P and T are temperature and pressure. Such mechanisms could explain the apparent high-attenuation zone in the upper mantle in terms of temperature and pressure variations alone; in the upper mantle the effect of temperature predominates and the internal friction is high, but in the lower mantle the effect of pressure suppresses this mechanism and the internal friction decreases. This type of mechanism gives a satisfactory fit to seismic surface-wave attenuation data, provided that the activation volume is relatively small (i.e., the pressure effect is weak). This mechanism assumes a frequency-independent internal friction, which is somewhat in conflict with experimental observations in oxides, but which will be justified below.

Anderson [1967] also reviewed some of the physical mechanisms likely to be important sources of attenuation in the earth and further emphasized the importance of the strong increase in internal friction observed at high temperature and its probable relation to grain boundary phenomena. Although noting the strong frequency dependence of most attenuation mechanisms, he pointed out

that a distribution of chemical and physical properties might weaken the frequency dependence, so that in a multicomponent, multiphase system with a spectrum of grain sizes, an internal friction which is only a weak function of frequency is not unexpected. *Savage* [1967] invoked a similar argument to give a frequency-independent Q^{-1} for a thermoelastic mechanism.

The present paper extends these earlier discussions of microscopic seismic loss mechanisms. Unfortunately, the conclusions cannot be definitive, since the loss mechanism is difficult to pin down even in the laboratory, where measurements can be made as a function of frequency, temperature, pressure, purity, grain size, annealing history, etc. Also, it is unfortunate that geophysicists on the one hand, and experimenters in physical and engineering properties of material on the other hand, have not asked the same questions about the anelastic properties of solids. Geophysicists are concerned with the relative attenuation of compressional and shear waves, attenuation at extremely low frequencies (10^{-4} to 1 Hz), and the effects of high temperature and pressure. Experimenters in other fields have been concerned largely with ultrasonic effects at low temperature and have done very little to investigate the effects of high pressure or the relative attenuation of compressional and shear waves. Most experimental measurements by geophysicists have been on rocks at low pressures, for which the attenuation is probably dominated by cracks and porosity, and which would be unrepresentative of mantle materials. Measurements by other experimenters have been performed on extremely pure materials of uniform composition and grain size, which, again, are probably not representative of mantle materials.

Much of what follows has been taken from the literature of applied physics, acoustics, mechanical engineering, metallurgy, ceramic science, and glass technology. Only the mechanisms that are likely to be relevant to attenuation at high temperature and pressure and to polycrystalline solids will be considered here. Rayleigh scattering, quantum mechanical effects, ferromagnetic, electron-phonon, and phonon-phonon interactions will not be considered, nor will a comprehensive review of data for metals, plastics, rubbers, purely ionic materials, or rocks at room temperature and pressure be attempted.

In reviewing the seismological and experimental observations of anelasticity, we shall depart from seismological tradition and refer to the property Q^{-1} rather than its inverse, Q, the quality factor. We do this for two reasons. First, a seismic wave traveling over regions of different anelastic properties is attenuated according to an average of the $(1/Q)$'s rather than the Q's. For body waves in a layered medium, the weighting factor for this average is the travel time in each layer; for surface waves and free oscillations, the weighting factor is related to the elastic energy. If the weighting factors for two layers are the same but the Q's are 100 and 1000, respectively, the 'average' Q will be 182. If the Q's are 100 and 10,000, the 'average' will be only 198. Thus Q can be a rather misleading measurement when it is used to represent an average of the properties of different regions.

Second, when attenuation is caused by more than one mechanism, the total attenuation will be described by the sum of the Q^{-1} from the separate mechanisms (provided that the mechanisms are linear and independent). This fact makes

curve fitting far easier when dealing wih Q^{-1}. In addition, Q^{-1} is a direct measure of anelasticity or departure from ideal elasticity and is more meaningful physically than is its inverse.

RECENT SEISMIC RESULTS

The seismic determinations of attenuation in the mantle have recently been summarized by *Knopoff* [1964] and *Anderson* [1967]. The discovery that the low-velocity zone in the upper mantle is also a region of high absorption is one of the most important results to date. Data from Love waves and Rayleigh waves suggest that attenuation in shear is greater than attenuation in compression [*Anderson et al.*, 1965]. No clear-cut evidence has yet been found for an intrinsic frequency dependence for Q^{-1}. Unfortunately, some assumptions about the frequency dependence of Q^{-1} are required in the surface-wave, free-oscillation, and spectral-ratio methods of estimating Q^{-1} in the various regions of the earth. Since highly absorptive regions in the upper mantle appear to dominate observed attenuations, it has not yet been possible to determine the details of the Q^{-1} variation with depth in the lower mantle. It is only possible to state that the average Q^{-1} of the lower mantle is about an order of magnitude lower than the average Q^{-1} of the upper mantle.

Press [1956], *Anderson and Kovach* [1964], and *Kovach and Anderson* [1964] determined average values of Q^{-1} for shear waves for the whole mantle that fell in the range 0.0017 to 0.0020 for shear waves of periods 10 to 50 sec. Using 1-sec P waves, *Kanamori* [1967*a*] concluded that Q_α^{-1} for 1-sec waves was nearly the same as Q_β^{-1} determined from much longer-period surface waves. *Otsuka* [1963] estimated Q_β^{-1} for the whole mantle to be 3.3×10^{-3} for 5-sec shear waves. *Hirasawa and Takano* [1966] determined an average Q^{-1} of 3.0×10^{-3} for P waves in the period range 3 to 30 sec. If $Q_\alpha^{-1} < Q_\beta^{-1}$ at a given period, as the surface-wave results suggest, there is a slight suggestion that Q^{-1} decreases with period. Table 1 summarizes available body-wave determinations of Q^{-1} in various regions of the earth. Surface-wave and free-oscillation determinations as a function of period are summarized in Table 2, guided waves in Table 3. Figure 1 displays Q^{-1} versus period for body waves, while Figure 2 does the same for surface waves and free oscillations.

TYPES OF MECHANISM

Apparent attenuation of elastic waves may result from geometrical effects or from actual loss mechanisms. Geometrical effects such as refraction, reflection, and scattering can be viewed as the result of the boundary conditions imposed on the wave-propagation problem, and do not reflect the anelastic properties of the propagating medium. Except for a few words about scattering, only the actual loss mechanisms will concern us here. These mechanisms may be categorized as follows:

Scattering. When the medium contains inhomogeneities comparable in scale to the wavelength of the elastic wave, then significant scattering will occur. The resulting attenuation is linear and highly frequency dependent. Although in principle this is a geometric mechanism, its effects cannot be computed and removed from seismic-amplitude data.

TABLE 1. Attenuation of Seismic Body Waves in the Mantle

Depth,* km	Period, sec	10000/Q	Q	Reference	Notes†
			P Waves		
Whole	4	8	1300	*Gutenberg*, 1945	
Whole	2	4	2500	*Gutenberg*, 1958	
Whole	12	25	400	*Gutenberg*, 1958	
Whole	0.14–0.3	2–5	2000–4000	*Asada and Takano*, 1963	
Whole	1	10	1000	*Carpenter*, 1964	
Whole	0.8–2.5	16–24	410–630	*Kanamori*, 1967*b*	SR
Whole	3–30	29	340	*Hirasawa and Takano*, 1966	SR
Whole	0.5–2.0	23	435	*Kanamori*, 1967*a*	SR
Upper		33–333	30–300	*Utsu*, 1966	1
Upper	0.1	5–20	500–2000	*O'Brien*, 1968	2
A 125	0.5	21	475	*Dorman*, 1968	
A 430		53–167	60–190	*Teng*, 1966	SR
A 870	0.8–2.5	42–56	180–240	*Kanamori*, 1967*c*	SR
A 920	3–30	71	140	*Hirasawa and Takano*, 1966	SR
B 870	0.8–2.5	2–6	1600–6000	*Kanamori*, 1967*c*	SR
B 920	3–30	4	2370	*Hirasawa and Takano*, 1966	SR
			S Waves		
Whole	11	20	500	*Press*, 1956	
Whole	12	14	700	*Gutenberg*, 1958	
Whole	24	25	400	*Gutenberg*, 1958	
Whole	5	33	300	*Otsuka*, 1963	
Whole	25	20	508	*Anderson and Kovach*, 1964	
Whole	25	23	440	*Anderson and Kovach*, 1964	
Whole	25	51	195	*Sato and Espinosa*, 1965	
Whole	90	114	88	*Sato and Espinosa*, 1965	
Whole	34	14	720	*Sato and Espinosa*, 1967	
Whole	90	43	232	*Sato and Espinosa*, 1967	
Whole	2–20	29	340	*Otsuka*, 1962	
Whole	2–20	27	370	*Otsuka*, 1962	
Whole	25–90	55	182	*Sato and Espinosa*, 1965	
Whole	25–38	17	581	*Sato and Espinosa*, 1967	
A 600		>62	<160	*Steinhart et al.*, 1964	
A 600	2–20	67	150	*Otsuka*, 1962	
A 600	25	66	151	*Anderson and Kovach*, 1964	
A 600	25	54	185	*Anderson and Kovach*, 1964	
A 1100	2–20	29	350	*Otsuka*, 1962	
B 600	25	7	1430	*Anderson and Kovach*, 1964	
B 600		<20	>500	*Steinhart et al.*, 1964	
Whole	14–67	17	600	*Kovach and Anderson*, 1964	SR
Whole	1.5–5.0	44	230	*Kanamori*, 1967*b*	SR
A 600	14–67	50	200	*Kovach and Anderson*, 1964	SR
B 600	14–67	5	2200	*Kovach and Anderson*, 1964	SR

* *A*, above; *B*, below.

† SR denotes measurement by spectral ratio of two different seismic phases. This method requires assumption that Q^{-1} is independent of period. Note 1, Japan; note 2, Lake Superior to Arizona.

TABLE 2. Attenuation of Seismic Surface Waves and Free Oscillations in the Mantle

Mode	Period	10,000/Q	Q	Reference
		Rayleigh Waves and Spheroidal Oscillations		
R	140	58	172	*Ewing and Press*, 1954*a*
R	215	53	189	*Ewing and Press*, 1954*a*
0S2	3230	27	370	*Alsop et al.*, 1961
0S2	3230	<33	>300	*Benioff et al.*, 1961
0S3	2133	26	380	*Benioff et al.*, 1961
0S0	1227	1.3	7500	*Ness et al.*, 1961
0S9	634	27	366	*Ness et al.*, 1961
0S12	502	36	280	*Ness et al.*, 1961
0S2	3230	29	350	*Smith*, 1961
R	125.0	66	151	*Anderson et al.*, 1965
R	114.6	63	158	*Anderson et al.*, 1965
R	104.2	62	160	*Anderson et al.*, 1965
R	96.2	66	152	*Anderson et al.*, 1965
R	89.3	69	145	*Anderson et al.*, 1965
R	73.5	76	132	*Anderson et al.*, 1965
R	62.5	81	123	*Anderson at al.*, 1965
R	54.3	84	119	*Anderson et al.*, 1965
R	52.1	83	121	*Anderson et al.*, 1965
R	50.0	80	125	*Anderson et al.*, 1965
R	333	38	265	*Anderson et al.*, 1965
R	294	45	222	*Anderson et al.*, 1965
R	263	48	209	*Anderson et al.*, 1965
R	238	51	195	*Anderson et al.*, 1965
R	217	54	184	*Anderson et al.*, 1965
R	200	59	176	*Anderson et al.*, 1965
R	185	59	169	*Anderson et al.*, 1965
R	172	60	167	*Anderson et al.*, 1965
R	161	60	166	*Anderson et al.*, 1965
R	151	61	164	*Anderson et al.*, 1965
R	333	55	183	*Ben-Menahem*, 1965
R	312	54	184	*Ben-Menahem*, 1965
R	278	56	178	*Ben-Menahem*, 1965
R	250	56	180	*Ben-Menahem*, 1965
R	227	56	180	*Ben-Menahem*, 1965
R	208	56	177	*Ben-Menahem*, 1965
R	192	57	176	*Ben-Menahem*, 1965
R	179	58	171	*Ben-Menahem*, 1965
R	167	61	164	*Ben-Menahem*, 1965
R	156	62	160	*Ben-Menahem*, 1965
R	147	65	155	*Ben-Menahem*, 1965
R	139	67	149	*Ben-Menahem*, 1965
R	132	68	146	*Ben-Menahem*, 1965
R	125	70	143	*Ben-Menahem*, 1965
R	114	63	158	*Ben-Menahem*, 1965
R	96.2	66	152	*Ben-Menahem*, 1965
R	83.3	72	138	*Ben-Menahem*, 1965
R	73.5	76	132	*Ben-Menahem*, 1965
R	65.8	79	127	*Ben-Menahem*, 1965
R	59.5	84	119	*Ben-Menahem*, 1965
R	54.3	84	119	*Ben-Menahem*, 1965

TABLE 2 (*continued*)

Mode	Period	10,000/Q	Q	Reference
R	50.0	80	125	*Ben-Menahem*, 1965
R	238	51	195	*Ben-Menahem*, 1965
R	217	54	184	*Ben-Menahem*, 1965
R	200	57	176	*Ben-Menahem*, 1965
R	185	59	169	*Ben-Menahem*, 1965
R	172	60	167	*Ben-Menahem*, 1965
R	161	60	166	*Ben-Menahem*, 1965
R	152	61	164	*Ben-Menahem*, 1965
R	217	54	185	*Ben-Menahem*, 1965
R	200	57	175	*Ben-Menahem*, 1965
R	185	68	148	*Ben-Menahem*, 1965
R	172	70	142	*Ben-Menahem*, 1965
R	161	74	136	*Ben-Menahem*, 1965
R	152	75	133	*Ben-Menahem*, 1965
R	143	76	132	*Ben-Menahem*, 1965
R	200	52–59	170–190	*Savarensky et al.*, 1966
1S3	1070	53	189	*Nowroozi*, 1968
1S5	728	51	195	*Nowroozi*, 1968
1S7	617	62	161	*Nowroozi*, 1968
0S10	580	43	233	*Nowroozi*, 1968
0S11	536	39	254	*Nowroozi*, 1968
0S12	502	41	242	*Nowroozi*, 1968
0S13	472	32	310	*Nowroozi*, 1968
0S14	449	40	252	*Nowroozi*, 1968
0S15	428	47	214	*Nowroozi*, 1968
0S16	411	45	224	*Nowroozi*, 1968
0S17	389	48	215	*Nowroozi*, 1968
0S18	376	46	219	*Nowroozi*, 1968
0S19	371	53	189	*Nowroozi*, 1968
0S20	354	30	330	*Nowroozi*, 1968
0S21	337	33	305	*Nowroozi*, 1968
0S23	314	34	291	*Nowroozi*, 1968
0S24	310	42	241	*Nowroozi*, 1968
0S0	1227	0.8	12000	*Slichter*, 1967
0S2	3230	20	500	*Slichter*, 1967
0S3	2133	19	520	*Slichter*, 1967
0S4	1551	25	400	*Slichter*, 1967
0S9	634	31	320	*Slichter*, 1967
0S12	502	50	200	*Slichter*, 1967
		Love Waves and Torsional Oscillations		
G	100	134	75	*Gutenberg*, 1924
Love	92	120	83	*Wilson*, 1940
Love	55	72	139	*Wilson*, 1940
Love	34	44	228	*Wilson*, 1940
Love	26	32	312	*Wilson*, 1940
G	360	110	91	*Sato*, 1958
G	216	76	132	*Sato*, 1958
G	108	84	119	*Sato*, 1958
G	72	77	130	*Sato*, 1958
G	54	58	172	*Sato*, 1958
G	43	39	256	*Sato*, 1958

TABLE 2 (*continued*)

Mode	Period	10,000/Q	Q	Reference
G	360	154	65	*Sato*, 1958
G	216	107	93	*Sato*, 1958
G	108	103	97	*Sato*, 1958
G	72	77	130	*Sato*, 1958
Love	60	49	202	*Popov*, 1960
0T5	1074	33	300	*Alsop*, 1961
0T8	741	40	250	*MacDonald and Ness*, 1961
0T10	674	50	200	*MacDonald and Ness*, 1961
G	400	89	112	*Press et al.*, 1961
G	200	97	103	*Press et al.*, 1961
G	100	77	130	*Press et al.*, 1961
G	300	120	83	*Bath and Lopez-Arroyo*, 1962
G	200	73	137	*Bath and Lopez-Arroyo*, 1962
G	150	74	135	*Bath and Lopez-Arroyo*, 1962
G	120	90	111	*Bath and Lopez-Arroyo*, 1962
G	86	100	100	*Bath and Lopez-Arroyo*, 1962
G	100	98	102	*Bath and Lopez-Arroyo*, 1962
G	76	94	106	*Bath and Lopez-Arroyo*, 1962
0T2	2599	25	400	*Smith*, 1961
0T3	1711	25	400	*Smith*, 1961
Love	125.0	92	109	*Anderson et al.*, 1965
Love	113.6	92	109	*Anderson et al.*, 1965
Love	104.2	88	114	*Anderson et al.*, 1965
Love	96.2	83	121	*Anderson et al.*, 1965
Love	89.3	78	128	*Anderson et al.*, 1965
Love	78.1	80	125	*Anderson et al.*, 1965
Love	69.4	95	106	*Anderson et al.*, 1965
Love	62.5	100	100	*Anderson et al.*, 1965
Love	56.8	99	101	*Anderson et al.*, 1965
Love	52.1	93	107	*Anderson et al.*, 1965
Love	50.0	90	111	*Anderson et al.*, 1965
Love	333	74	135	*Anderson et al.*, 1965
Love	312	74	135	*Anderson et al.*, 1965
Love	294	74	135	*Anderson et al.*, 1965
Love	278	76	132	*Anderson et al.*, 1965
Love	263	77	130	*Anderson et al.*, 1965
Love	250	76	131	*Anderson et al.*, 1965
Love	227	75	133	*Anderson et al.*, 1965
Love	208	76	131	*Anderson et al.*, 1965
Love	192	76	131	*Anderson et al.*, 1965
Love	178	77	130	*Anderson et al.*, 1965
Love	167	77	130	*Anderson et al.*, 1965
Love	156	79	127	*Anderson et al.*, 1965
Love	71.4	92	109	*Ben-Menahem*, 1965
Love	69.4	93	108	*Ben-Menahem*, 1965
Love	65.8	96	104	*Ben-Menahem*, 1965
Love	62.5	100	100	*Ben-Menahem*, 1965
Love	59.5	100	100	*Ben-Menahem*, 1965
Love	56.8	99	101	*Ben-Menahem*, 1965
Love	73.5	89	112	*Ben-Menahem*, 1965
Love	65.8	99	101	*Ben-Menahem*, 1965
Love	59.5	100	100	*Ben-Menahem*, 1965

TABLE 2 (*continued*)

Mode	Period	10,000/Q	Q	Reference
Love	54.3	97	103	*Ben-Menahem*, 1965
Love	50.0	90	111	*Ben-Menahem*, 1965
Love	125	95	105	*Ben-Menahem*, 1965
Love	114	94	106	*Ben-Menahem*, 1965
Love	104	94	107	*Ben-Menahem*, 1965
Love	96	94	107	*Ben-Menahem*, 1965
Love	91	94	107	*Ben-Menahem*, 1965
Love	83	93	108	*Ben-Menahem*, 1965
Love	78	93	108	*Ben-Menahem*, 1965
Love	74	93	108	*Ben-Menahem*, 1965
Love	278	68	148	*Ben-Menahem*, 1965
Love	263	70	143	*Ben-Menahem*, 1965
Love	238	70	143	*Ben-Menahem*, 1965
Love	217	70	143	*Ben-Menahem*, 1965
Love	200	71	141	*Ben-Menahem*, 1965
Love	185	74	135	*Ben-Menahem*, 1965
Love	172	79	126	*Ben-Menahem*, 1965
Love	161	86	117	*Ben-Menahem*, 1965
Love	152	89	113	*Ben-Menahem*, 1965
Love	143	90	111	*Ben-Menahem*, 1965
Love	200	76	131	*Ben-Menahem*, 1965
Love	185	77	130	*Ben-Menahem*, 1965
Love	172	77	130	*Ben-Menahem*, 1965
Love	161	79	127	*Ben-Menahem*, 1965
Love	152	79	127	*Ben-Menahem*, 1965
Love	217	68	146	*Ben-Menahem*, 1965
Love	200	75	134	*Ben-Menahem*, 1965
Love	185	78	129	*Ben-Menahem*, 1965
Love	172	82	122	*Ben-Menahem*, 1965
Love	161	85	117	*Ben-Menahem*, 1965
Love	152	88	114	*Ben-Menahem*, 1965
Love	143	90	111	*Ben-Menahem*, 1965
Love	135	94	106	*Ben-Menahem*, 1965
Love	128	94	106	*Ben-Menahem*, 1965
Love	125	96	104	*Ben-Menahem*, 1965
Love	300	100	100	*Savarensky et al.*, 1966
Love	400	100	100	*Savarensky et al.*, 1966
Love	450	91	110	*Savarensky et al.*, 1966
Love	500	167	60	*Savarensky et al.*, 1966
Love	250	67	150	*Savarensky et al.*, 1966
Love	300	77	130	*Savarensky et al.*, 1966
0T8	735	43	232	*Nowroozi*, 1968
0T9	670	64	157	*Nowroozi*, 1968
0T10	619	43	234	*Nowroozi*, 1968
0T12	537	67	150	*Nowroozi*, 1968
0T13	500	53	190	*Nowroozi*, 1968
0T14	474	74	135	*Nowroozi*, 1968
0T17	408	79	126	*Nowroozi*, 1968
0T18	390	37	270	*Nowroozi*, 1968
0T19	374	36	281	*Nowroozi*, 1968
0T21	346	59	170	*Nowroozi*, 1968

TABLE 3. Attenuation of Guided Waves in the Mantle*

Mode	Period	10,000/Q	Q
PG	0.81	55	180
PG	0.52	38	260
PG	0.82	75	134
PG	0.83	24	410
PG	0.68	49	205
PG	0.76	29	340
PG	0.76	36	276
LG	1.4	23	430
LG	0.64	23	440
LG	1.1	20	510
LG	0.82	16	610
LG	0.84	26	380
LG	0.80	27	370
LG	0.8	24	415

* Values taken from *Press* [1964].

Damped resonance. If in a solid there is a restoring force on an internal point proportional to its relative velocity, then the work done against the restoring force is converted to heat, and internal friction occurs. This internal friction is linear and frequency dependent.

Static hysteresis. When stress causes a change in the condition of the solid that is not reversed upon reversal of the stress (*e.g.*, frictional heating), 'static hysteresis' internal friction results. The internal friction is amplitude dependent, and therefore nonlinear, and in many cases is independent of frequency. As for all anelastic mechanisms, the stress-strain curve will be a 'hysteresis loop,' but for static hysteresis, this loop persists to very low frequencies (i.e., until the period of the stress cycle approaches the time required to anneal out the stress-induced damage). For other mechanisms, the hysteresis loop will close at low frequencies.

Relaxation. When stress causes a change in the condition of the solid that is reversed upon reversal of the stress (e.g., thermoelastic heating, phase changes, short excursions of defects), 'relaxation' takes place. This process acts to relieve the instantaneous stress, causing linear, frequency-dependent, internal friction.

Viscosity. Another type of internal friction is attributed to 'viscosity.' When applied to solids, this term usually means that stress relief and deformation occur by some poorly understood process, which may be a combination of several types of processes, and may result in linear or nonlinear internal friction of complicated (or unknown) frequency dependence.

DAMPED RESONANCE MECHANISMS

Forced resonance of dislocations in their equilibrium potential wells can contribute to the damping of waves with frequencies comparable to the resonant frequency of the pinned dislocation segments. It has been proposed [*Granato and Lücke*, 1956] that a pinned edge dislocation may act as a violin string with a damping

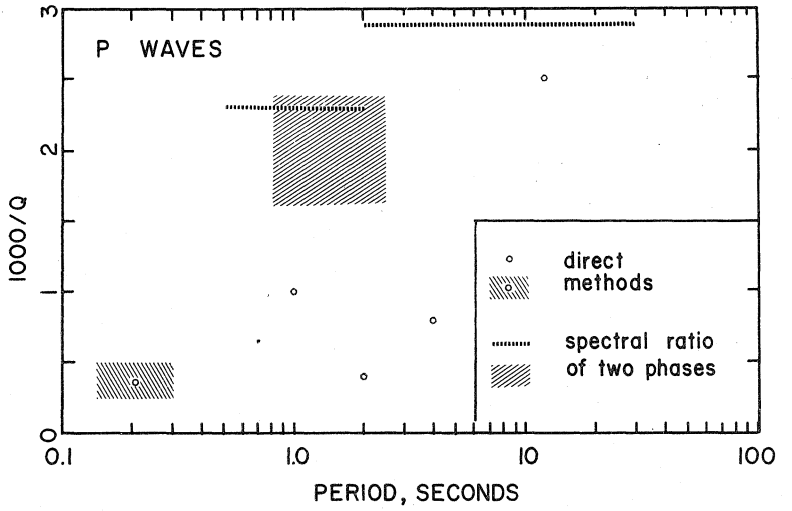

(a)

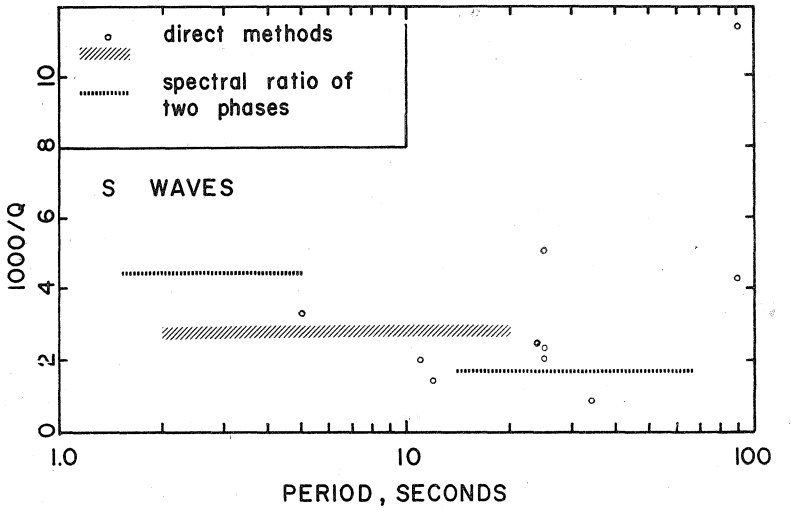

(b)

Fig. 1. Internal friction in the earth as a function of period (*top*) measured by seismic P waves and (*bottom*) measured by seismic S waves. The methods involving the spectral ratio of two phases rely on the assumption that Q^{-1} is independent of period over the range of periods studied, and the reported value reflects some weighted 'average' of the Q^{-1} of the mantle, which is difficult to interpret unless the mantle is assumed to have a uniform Q^{-1}.

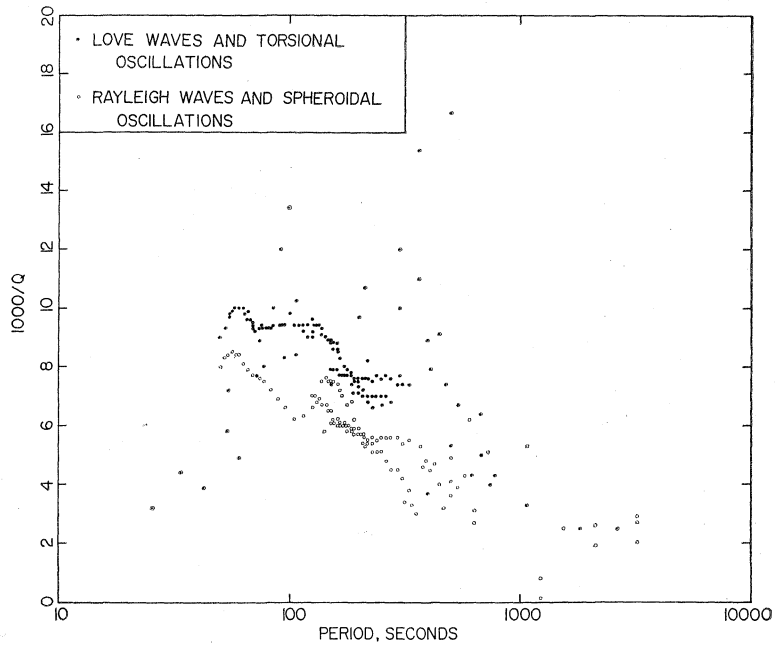

Fig. 2. Damping of seismic surface waves and free oscillations.

force proportional to its velocity. The dislocation motion is described by $m\ddot{x} + \beta\dot{x} + kx = Fe^{i\omega t}$, where x is the normal displacement from the equilibrium position, m is some constant representing the 'effective mass' of the dislocation, β is the restoring force per unit velocity, k is the 'spring constant,' and F and ω are the amplitude and frequency of the driving force, which in this case would be a passing shear wave. The internal friction is then [*Van Bueren*, 1961]

$$Q^{-1} = \frac{\omega\beta/m}{[(\omega_0^2 - \omega^2)^2 + (\omega^2\beta^2/m^2)]^{1/2}}$$

where $\omega_0 = (k/m)^{1/2}$, the resonant frequency. For $\omega \ll \omega_0$, $Q^{-1} = \omega\beta/m\omega_0^2$ [*Van Bueren*, 1961]. This mechanism would directly affect only shear waves, but, because of stress inhomogeneities, it would also attenuate compressional waves to a smaller extent.

The parameters ω_0 and β will depend on the dislocation loop length, so that the internal friction for the whole sample must be found by integrating over all loop lengths. It is often assumed [*Niblett and Wilks*, 1960] that the number of loops per unit volume with lengths between l and $l + dl$ is

$$N(l)dl = (\Lambda/L^2) \exp(-l/L)dl \qquad (1)$$

where Λ is the dislocation density and L is the average loop length. The units of $N(l)$ are cm^{-4}, while Λ is in cm^{-2}, and L is in cm. The loop length will be determined by the number of pinning points per unit volume, n (in cm^{-3}), so that

$$N(l) = (n^2/\Lambda) \exp(-nl/\Lambda)$$

When the integration is performed,

$$Q^{-1} = C_1 \Lambda L^4 \frac{\beta\omega}{\mu b^3}\left[1 + C_2 L^2 \frac{m\omega^2}{\mu} - C_3 L^4 \frac{\beta^2\omega^2}{\mu^2 b^2}\right]$$

[*Van Bueren*, 1961], where C_1, C_2, C_3 are numerical constants between 1 and 10, μ is the shear modulus, and b is the Burgers vector. It can be seen that Q^{-1} is strongly dependent on average loop length and Q^{-1} is proportional to Λ. Generally speaking, the internal friction will increase with temperature, as thermal unpinning will increase the average loop length, even though some dislocations will anneal out at high temperature, resulting in a decrease in Λ. Q^{-1} decreases with radiation damage and point-defect concentration, as these decrease the average loop length.

The damped resonance of dislocations has been used to explain the internal friction at megacycle frequencies, which could not be explained in other ways. Data for Si, Ge, Pb, Cu, Al, Zn, and NaCl have been fitted with this model, but, because of the large number of adjustable parameters involved, the interpretation is not unique. Since this mechanism appears only at high frequencies and invokes a velocity-dependent damping force which is difficult to justify, we shall not consider it further. It has not been observed in silicates or oxides.

STATIC HYSTERESIS MECHANISMS

Sliding Friction across Cracks

The dissipation of energy by friction across cracks has been treated by *Walsh* [1966]. This mechanism adequately explains measurements on rocks at low pressures, including the frequency independence of the internal friction and its decrease with pressure [*Birch*, 1938]. The mechanism requires partially closed cracks, held together loosely enough so that low seismic shear stresses (less than 1 bar) will cause slippage, and requires further that the two surfaces of the crack remain in contact. Under very modest pressures (about 10 kbar), all cracks in dry rocks would effectively be closed, and this mechanism would not operate. In wet or partially molten rocks, a thin film of fluid might act to relieve overburden pressure and keep cracks open or at least lubricated. Relative motion may occur across grain boundaries at high pressure, especially in the presence of water, a partial melt, or some other fluid, but here the attenuation is much more likely to result not from sliding friction but from a quasi-viscous stress relaxation. These mechanisms will be covered in detail in later sections. It is our conclusion that sliding friction may very well account for most of the internal friction measured in rocks in the laboratory but is unlikely to cause significant attenuation of seismic waves in the mantle.

Granato-Lücke Dislocation Hysteresis

Granato and Lücke [1956] proposed that an applied shear stress can tear dislocations irreversibly away from impurity atoms or other point defects where they are normally pinned by an attractive force. The stress required to accom-

plish such unpinning is inversely proportional to the length of a dislocation segment between pinning points. Thus the process is catastrophic; once a dislocation segment is torn from an interior pinning point, its effective length increases, and very little stress is needed to pull it entirely free of other pinning points. This mechanism is dependent on amplitude and is inoperative below the threshold strain necessary to unpin the first short dislocation segment. If the number of pinned segments of length l is given by $N(l)\ dl = (\Lambda/^2)\exp(-l/L)dl$ as above, then the theory predicts that

$$Q^{-1} = (Aa/L^2\epsilon)\ \exp\ (-\ Ba/L\epsilon)$$

where A and B are constants depending on orientation and dislocation density, a is the lattice spacing, and ϵ is the strain amplitude [*Niblett and Wilks,* 1960, p. 42]. The predicted amplitude dependence will be modified if a different length distribution is assumed. The theory predicts no explicit frequency dependence.

Observations attributed to this type of internal friction in metals exhibit the following properties [*Niblett and Wilks,* 1960]:

1. The internal friction decreases with time, but increases to its original value after annealing allows repinning of the dislocations.
2. The internal friction is increased by moderate amounts of cold work.
3. Large amounts of cold work cause the internal friction to decrease again, presumably because of strain hardening.
4. The presence of impurities reduces the internal friction.
5. The internal friction may depend on frequency. For zinc, Q^{-1} is proportional to $1/f$ [*Niblett and Wilks,* 1960]. For copper, *Kamentsky* [1957] found Q^{-1} increases with frequency.
6. The same mechanism causes a reduction in the elastic modulus proportional to Q^{-1}.
7. For low temperatures, Q^{-1} increases with increasing temperature, as thermal vibration contributes to the unpinning process and the equilibrium concentration of impurities decreases.
8. For high temperatures, the internal friction becomes very low because the thermal energy is great enough that nearly all dislocations are unpinned.

In addition to large amounts of data for metals [*Niblett and Wilks,* 1960], data on the Granato-Lücke dislocation hysteresis exist for single-crystal quartz, MgO, and TiO_2 (see Table 4). Figure 3 shows the internal friction in cold-worked MgO as a function of inverse temperature, illustrating effect 8 above.

This effect places in doubt the importance of the Granato-Lücke hysteresis mechanism in the mantle: the high temperature in the mantle is likely to have annealed out most dislocations and caused those remaining to be thermally unpinned already, unless the retarding effect of pressure is greater than seems likely. However, because the dislocation density in the mantle is unknown, and because the effect of pressure on thermal unpinning is not known, this mechanism should not be ruled out entirely without further experimentation.

TABLE 4. Granto-Lücke Hysteresis in Silicate and Oxide Single Crystals

Material	T, °K	f, Hz	Mode	$(Q^{-1})_{max}$	Threshold Strain	Reference
Natural quartz	300	6.4×10^4	Long.	5×10^{-4}	10^{-5}	*Hiki*, 1960
Synthetic quartz	300	6.4×10^4	Long.	6×10^{-5}	10^{-5}	*Hiki*, 1961
MgO	300	5	Flex.	10^{-2}	10^{-5}	*Dahlberg et al.*, 1962
MgO	80–1000	9×10^3	Long.	2×10^{-4}	2×10^{-6}	*Southgate et al.*, 1966
MgO	80–1000	9×10^4	Long.	2×10^{-4}	2×10^{-6}	*Southgate et al.*, 1966
TiO_2	187–577	3–5	Flex.	1.2×10^{-2}		*Carnahan and Brittain*, 1966

RELAXATION MECHANISMS

Such processes as thermoelasticity, diffusional motion of dislocations and point defects, stress-induced ordering, fluid flow in pores, phase changes, and twinning-detwinning of crystals, will act to relieve an applied stress. During one-half of a stress cycle energy is absorbed, and during the next half cycle energy

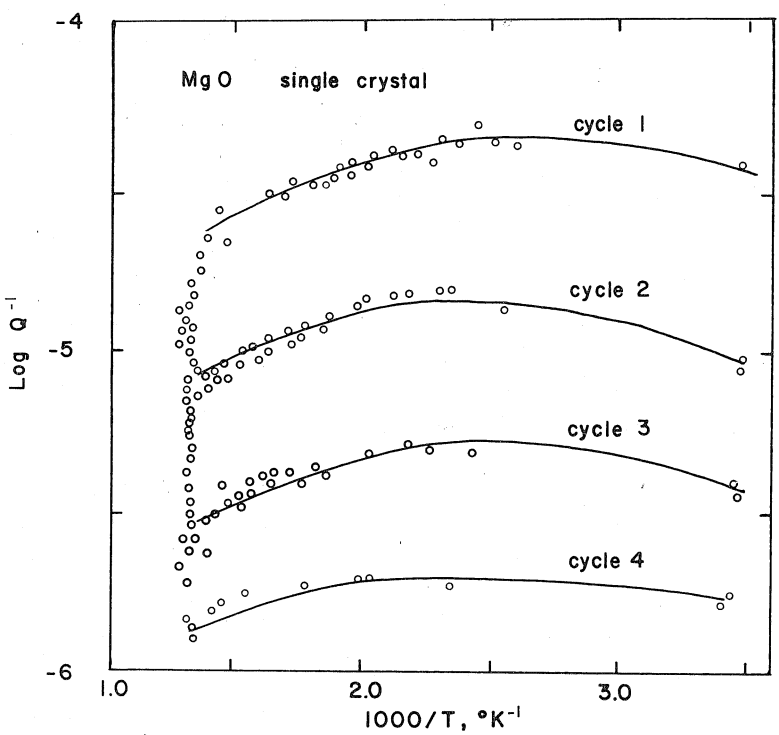

Fig. 3. Granato-Lücke amplitude-dependent internal friction in MgO. Repeated temperature cycles show strongly decreasing internal friction as dislocations become unpinned. Above 700°K, most dislocations are unpinned by thermal vibrations and the internal friction is very low [*Southgate et al., 1966*].

is given up. Usually a finite amount of time is required for this energy exchange to take place; this is called the relaxation time and tends to make strain out of phase with the applied stress. *Zener* [1948] assumed that for all these mechanisms the rate of stress relief for constant strain is proportional to the stress (a good assumption for small strains) and showed that each of the above mechanisms contributes an internal friction of the form

$$Q^{-1} = \frac{M_U - M_R}{M_U} \frac{f/f_p}{1 + (f/f_p)^2} \tag{2}$$

which is shown in Figure 4. Here M_U is an 'unrelaxed' elastic modulus, M_R is a smaller 'relaxed' modulus, and f_p is the constant of proportionality between the stress and the rate of stress relaxation. Notice that the maximum internal friction occurs at $f = f_p$. This mechanism will also be responsible for transient creep under constant stress:

$$\epsilon(t) = \frac{\sigma_0}{M_R}\left[1 - \frac{M_U - M_R}{M_U} \exp(-2\pi f_p t)\right]$$

where $\epsilon(t)$ is the strain as a function of time, and σ_0 is the stress. Thus

$$\dot{\epsilon}(t) = \frac{2\pi f_p \sigma_0}{M_R} \frac{M_U - M_R}{M_U} \exp(-2\pi f_p t)$$

The relaxation time for thermally activated mechanisms is dependent on both temperature and pressure. An isothermal relaxation process under conditions of constant pressure will require a 'free energy of activation,' $G^* = H^* - S^*T$, where H^* and S^* are the activation enthalpy and entropy. From statistical mechanical considerations, the relaxation time τ is given by

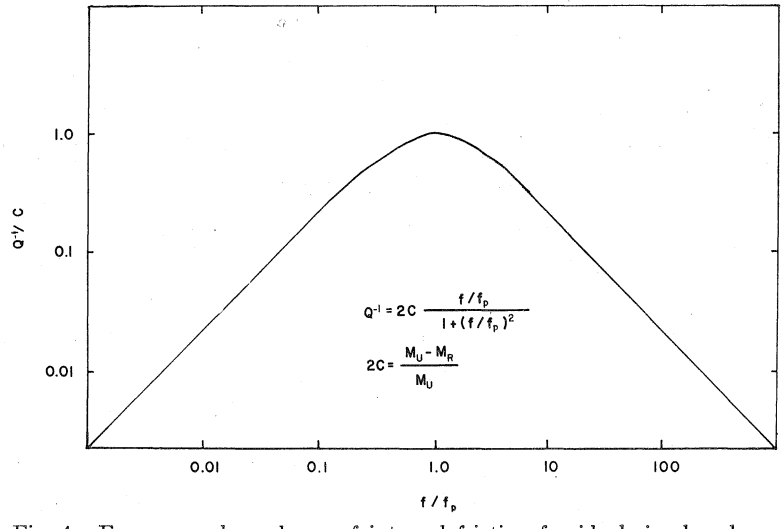

Fig. 4. Frequency dependence of internal friction for ideal simple relaxation mechanism, normalized by the peak height. A distribution of relaxation times will broaden the relaxation peak.

$$\tau = \tau_0 \exp (G^*/RT) = \tau_0 \exp (-S^*/R) \exp (H^*/RT) \tag{3}$$

where τ_0 is a constant and R is the gas constant. But $H^* = E^* + PV^*$, where E^* and V^* are the activation energy and activation volume. Thus if we know $\tau_0 \exp(-S^*/R)$, E^*, and V^*, and assume that they are effectively independent of temperature and pressure, we can specify τ at any temperature and pressure. From measurements of τ as a function of temperature and pressure, we obtain

$$H^* = R \frac{\partial \ln \tau}{\partial (1/T)} \qquad E^* = H^* \mid_{P=0} \qquad V^* = \frac{\partial H^*}{\partial P} \tag{4}$$

The constant $\tau_0 \exp(-S^*/R)$ can be obtained by extrapolating a plot of τ versus $1/T$ to the $1/T = 0$ axis. The peak frequency is given by

$$f_p = \frac{1}{2\pi\tau} = f_0 \exp (-H^*/RT) \tag{5}$$

where $f_0 = (1/2\pi\tau_0) \exp (S^*/R)$, and, as above, $H^* = E^* + PV^*$. These relations imply that, for a given relaxation with a single activation energy, $\log f_p$ is a linear function of $1/T$ with H^* given by the slope. This relationship is demonstrated in Figure 5, with selected values of f_0, E^*, and V^*, and a range of values of P.

Putting the expression for f_p into the equation for Q^{-1}, we find

$$Q^{-1} = \frac{M_U - M_R}{M_U} \frac{f/f_0 \exp (-H^*/RT)}{1 + [f/f_0 \exp (-H^*/RT)]^2} \tag{6}$$

A sample plot of Q^{-1} versus $1/T$ is shown in Figure 6. A consequence of equation 6 is that a thermally activated relaxation peak can be scanned experimentally over a small range of temperature rather than a wide range of frequency.

Thermoelastic Internal Friction

The best known classical relaxation mechanism is thermoelasticity. If no heat enters or leaves an element of material during its alternate cooling and heating due to a sound wave, and if the state of the material can be completely described by two independent local thermodynamic parameters such as T and P, the changes in pressure and density take place reversibly, and there is no attenuation. Otherwise, the pressure-density cycle is irreversible and some of the sound energy is transferred to random thermal energy. This results in both absorption and dispersion.

Variation of strain in a body is attended by variation of temperature which, in turn, causes a flow of heat. This gives rise to an increase in entropy and, consequently, to dissipation of vibrational energy. This process is not thermally activated and therefore the attenuation is not a strong function of temperature and pressure. In a homogeneous isotropic material there is no compression and, therefore, no temperature change during the passage of a transverse wave. Thermal conduction, therefore, cannot contribute to the absorption of shear waves in such a material. For compressional or longitudinal waves, the maximum damping occurs for periods of vibration that are comparable to the relaxation time. The

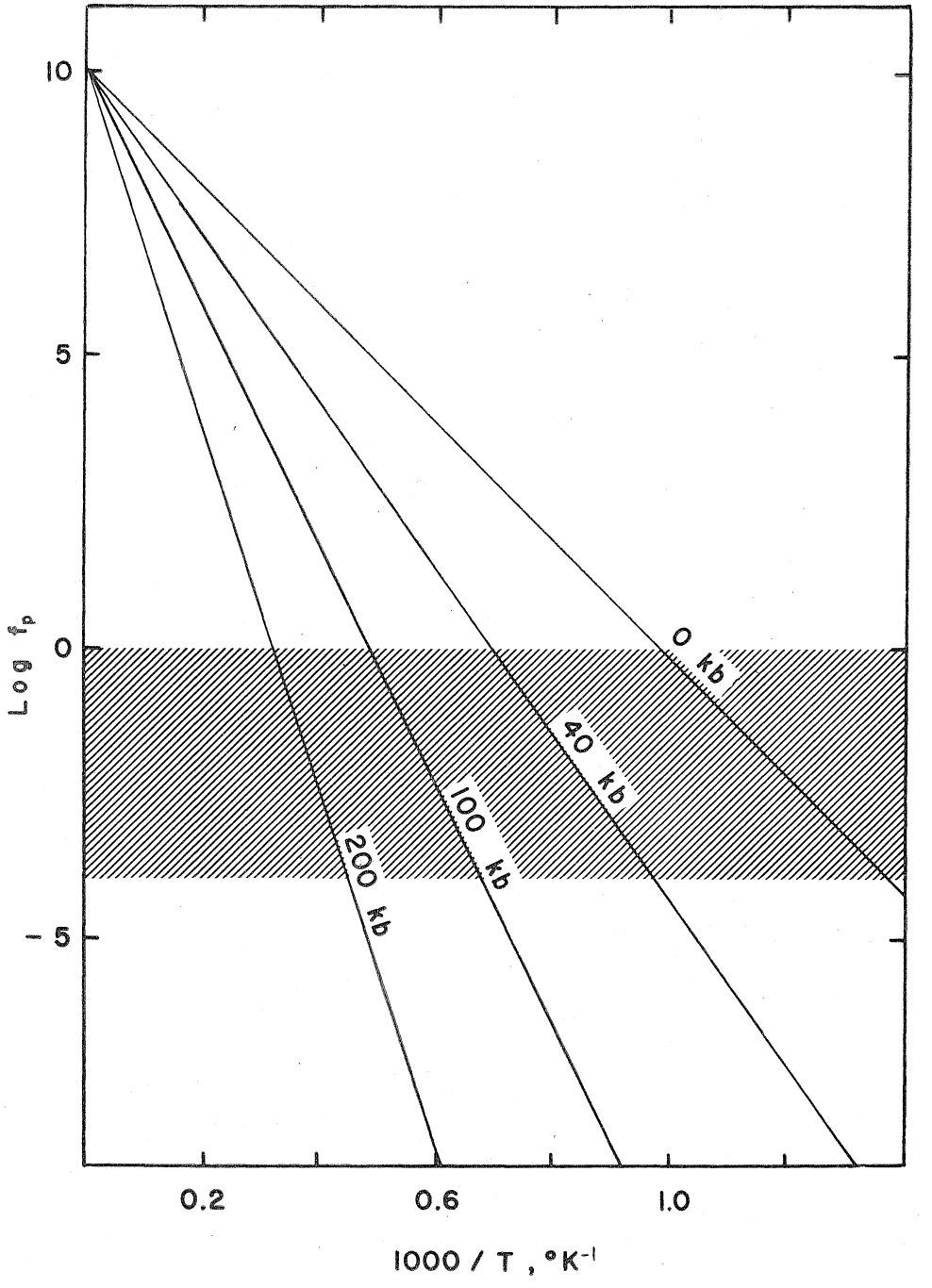

Fig. 5. Temperature dependence of relaxation peak frequency for several pressures, assuming $f_0 = 10^{10}$ Hz, $E^* = 47$ kcal/mole, and $V^* = 10$ cm^3/mole. Shaded region shows approximate range of frequencies of seismic interest.

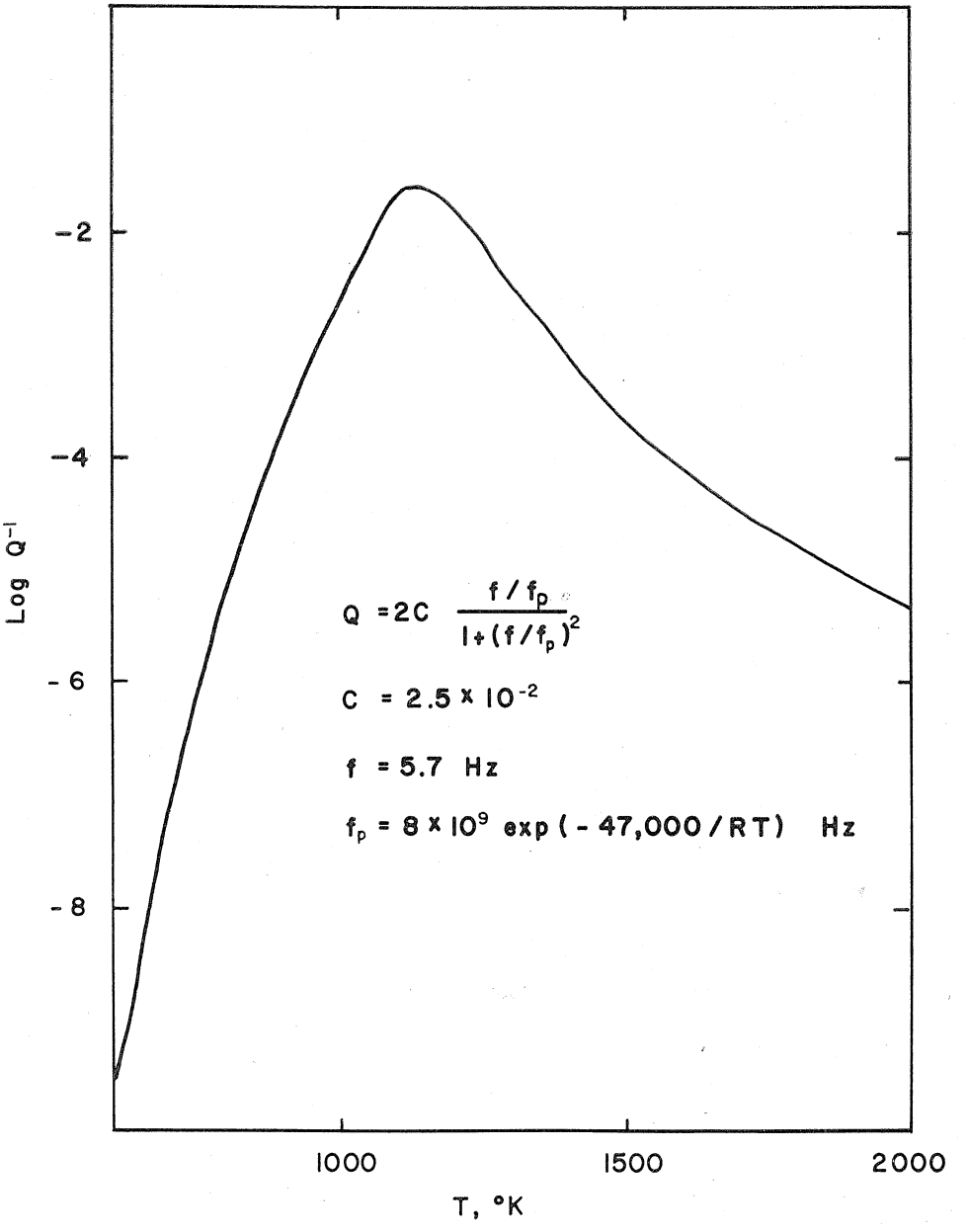

Fig. 6. Temperature dependence of internal friction assuming an ideal simple relaxation mechanism, the parameters being selected as shown. With these parameters, maximum damping would occur in the uppermost part of the mantle.

time required for the establishment of thermal equilibrium is proportional to the square of the distance a between regions of compression and dilatation, divided by the thermal diffusivity D. The peak frequency f_p is proportional to D/a^2 and is only slightly dependent on temperature. When the temperature must relax from the peak to the valley of a compressional wave, $a = \lambda/2 = V_p/2f$, where V_p is the compressional velocity, giving $f_p = 4Df^2/V_p^2$. The peak internal friction occurs for $f/f_p = 1$, or $f_p = V_p^2/4D = 10^{13}$ Hz for forsterite, far outside the range of seismic interest. Because the relaxation frequency f_p is dependent on the frequency of elastic wave f, we have the interesting relations that

$$\text{if } f \gg V_p^2/4D \quad \text{then} \quad f \ll f_p \qquad \text{(relaxed, or isothermal case)}$$

$$\text{if } f \ll V_p^2/4D \quad \text{then} \quad f \gg f_p \qquad \text{(unrelaxed, or adiabatic case)}$$

Thus low-frequency elastic waves ($f < 10^{13}$ Hz) are adiabatic, and only very-high-frequency waves would be isothermal. This is contrary to intuition, as one would expect high-frequency waves to be adiabatic and low-frequency waves to be isothermal. In static compression experiments the thermal relaxation distance a is no longer ½ the wavelength but is a constant depending on the geometry of the sample. These tests do measure isothermal properties. Both ultrasonic and seismic waves are adiabatic, and we have

$$Q^{-1} \cong \frac{M_U - M_R}{M_U} \frac{f_p}{f} = \frac{C_p - C_V}{C_p} \frac{4Df}{V_p^2}$$

As was noted above, $V_p^2/4D \cong 10^{13}$ Hz for forsterite (and is not much different for other solids). Because the seismic frequencies of interest in this paper are less than 1 Hz, we would expect negligible attenuation ($Q^{-1} < 10^{-13}$) in the mantle due to bulk thermoelastic attenuation.

Losses Due to Intergranular Thermal Currents

In a polycrystalline material there are local stress fluctuations, and therefore temperature fluctuations, associated with the heterogeneity or anisotropy of the grains. As in the case of bulk thermoelasticity, the temperature fluctuations will arise out of compressional strain only, and thus this mechanism will act directly upon compressional waves only. However, local stress inhomogeneities will cause this mechanism to attenuate shear waves also, but the effect will be less than for compressional waves. These temperature perturbations attempt to relax, but the diffusion distance is now only of the order of the grain size rather than of the wavelength.

Because of the imposition of boundary conditions at the grain surfaces, the equation given above for the relaxation-type internal friction no longer holds. *Randall et al.* [1939] showed that the frequency dependence of internal friction will be given by a function of the dimensionless normalized frequency fa^2/D only. Again, D is the thermal diffusivity, and a is the thermal relaxation distance, in this case approximately equal to the average grain diameter. *Zener and Randall* [1940] showed that, in the high-frequency limit, $fa^2/D \gg 1$, Q^{-1} is proportional to $1/(fa^2/D)^{1/2}$, whereas in the low-frequency case, Q^{-1} varies as

fa^2/D. This behavior was verified for α brass by *Randall et al.* [1939]; their results are shown in Figure 7. Note that $f_p \cong 6D/a^2$. For intergranular thermoelastic relaxation, we should have $(M_U - M_R)/M_U = (M_S - M_T)R/M_S$, where M_U is the unrelaxed elastic modulus, M_R is the relaxed elastic modulus, M_S is the adiabatic modulus, M_T is the isothermal modulus, and R is a factor to allow for the anisotropy in elastic modulus and coefficient of thermal expansion. The problems of the best measure to use for R and the form of the Q^{-1} versus f curve near the peak have never been solved for the general case where both the thermal expansion and the elastic constants are anisotropic. According to *Zener* [1948], R should be the variance over all orientations of the reciprocal elastic modulus for the case in which the thermal expansion coefficient is isotropic. However, using Zener's value of 0.091 for the anisotropy, and $(M_U - M_R)/M_U = E_S \cdot T\alpha_V^2/9C_V = 3.6 \times 10^{-3}$, the peak internal friction measured for α brass, as shown in Figure 7, is lower than the theoretical value by a factor of 2. In the equation above, E_S is the adiabatic Young's modulus, and α_V is the volume coefficient of thermal expansion. If we take $(M_U - M_R)/M_U = (C_p - C_V)/C_p = 2.7 \times 10^{-2}$ [*Mason*, 1958], the discrepancy between calculated and observed values is a factor of 14.

Unfortunately, the intergranular thermoelastic attenuation has not been identified experimentally either in rocks or in polycrystalline ceramics. Because of the ambiguities in the theory and in the experimental evidence in metals, the problem of scaling the data on metals to estimate the effect of this mechanism in the mantle is very difficult. If we accept the frequency scaling relation, i.e., f enters only in the dimensionless form fa^2/D, and use the empirical observation that in metals the maximum internal friction occurs when $fa^2/D \approx 6$, we can

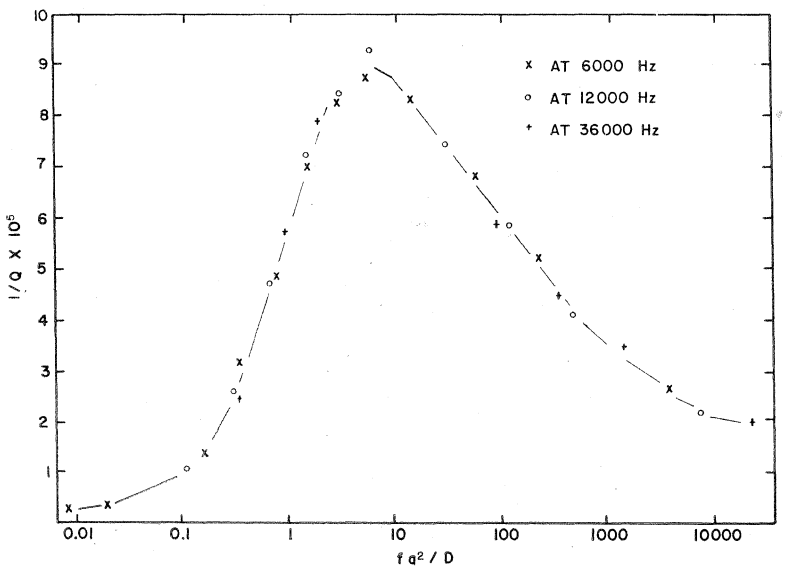

Fig. 7. Dependence of Q^{-1} on the parameter fa^2/D for α brass [*Randall et al.*, 1939]. The mechanism is presumed to be intergranular thermoelastic relaxation.

TABLE 5. Frequency Dependence of Thermoelastic Attenuation as a Function of Grain Size in Forsterite

$(Q^{-1})_{peak} \doteq 10^{-4}$ $f_p \doteq D/(gs)^2$

Grain Size, cm	Peak Frequency, cps
10^{-2}	10^{3}
10^{-1}	10
1	10^{-1}
10	10^{-3}
10^{2}	10^{-5}

estimate the frequency of maximum attenuation in the mantle for any assumed grain size. Table 5 shows the peak frequency expected for a range of possible grain sizes. The maximum internal friction will occur in the range of seismic frequencies if the grain size in the mantle is in the range of 1 to 100 cm. The magnitude of the peak internal friction is harder to estimate. Previous experiments have been performed primarily on cubic metals with isotropic coefficients of thermal expansion, so that the anisotropy factor R has reflected only the elastic anisotropy. In rocks, particularly multicomponent rocks, anisotropy of thermal expansion will be significant and the elastic anisotropy will probably exceed that of metals. The effect of variations in grain size in rocks would be to weaken the frequency dependence of the internal friction. Taking these effects into account, it has been estimated that the internal friction from this mechanism could reach 10^{-3} to 10^{-2} in the mantle [*Savage,* 1966; *Anderson,* 1967]. For shear waves, the attenuation would probably be somewhat less, but could still be significant. Substantial shear strains can be introduced in a heterogeneous solid by a purely longitudinal applied stress.

Bordoni Dislocation Relaxation

According to dislocation theory [*Van Bueren,* 1961], dislocations tend to lie in 'Peierls potential wells' parallel to closely packed rows of atoms in the slip planes. At sufficiently high temperatures, a segment of a dislocation may hop over one row of atoms into the next well, causing a double kink. If there were no stress, these kinks would tend to attract and annihilate one another, but an applied shear stress may drive them apart and cause deformation, relief of stress, and hence internal friction. For small enough stress, the process will be reversible, and the second half of the stress cycle will drive the kinks back together. The peak internal friction occurs at the frequency of thermal formation of kinks, which is given by [*Donth,* 1957]

$$f_p = \frac{\pi^2 GbkT}{32a^2 V_S{}^2 M^{3/2} E_0{}^{1/2}} \exp\left[F(W_k, T)\right]$$

where G is shear modulus.
a is lattice spacing.
b is Burgers vector.

V_S is shear velocity.
m is 'mass' of dislocation per unit length.
E_0 is dislocation energy per unit length.
W_k is energy of kink formation.
F is a function roughly proportional to $-2W_k/kT$.

It can be seen that f_p increases as T increases, roughly as $kT \exp(-2W_k/kT)$. The maximum internal friction is then

$$(Q^{-1})_{max} = b^2L^3N_0G/48E_0$$

where L is average length of dislocation loop, and N_0 is number of dislocations per square centimeter. Both f_p and $(Q^{-1})_{max}$ will depend strongly on the properties of the material and the history of the sample tested. Observations of this type of internal friction generally show [*Niblett and Wilks*, 1960] the following relations:

1. Cold work increases the internal friction, while annealing decreases it.
2. The internal friction is independent of strain amplitude.
3. Radiation damage and the presence of impurities reduce the internal friction.

The Bordoni relaxation has been observed in face-centered-cubic metals at temperatures less than 100°K and frequencies in the kilocycle to megacycle range [*Van Bueren*, 1961; *Niblett and Wilks*, 1960]. It does not appear in metals of more complicated structure, presumably because the mobility of the kinks is limited by the geometry of the crystal. Bordoni relaxations have also been cited as the cause of internal friction peaks in quartz, MgO, and Al_2O_3, as Table 6 shows.

Chang's [1961] data for cold-worked Al_2O_3 are shown in Figure 8. The alleged Bordoni peaks are superimposed on monotonic increases to be discussed below. Because all other observations of the Bordoni peak occur at less than room temperatures and at frequencies greater than 1000 Hz, the interpretation of the peaks in Chang's data as Bordoni relaxations must be viewed with some suspicion. Nevertheless, the peaks shown in Figure 8 are thermally activated relaxations associated with dislocations, and certainly have possible geophysical significance.

Huber et al. [1961] noticed a sharp increase above 1700°K in the internal friction of highly deformed Al_2O_3 single crystals vibrated longitudinally at about 50 kHz. This increase did not occur in undeformed samples. Thus the increase is

TABLE 6. Bordoni Relaxation in Oxide Single Crystals

Sample	f, Hz	T_p, °K	$Q^{-1}{}_{peak}$	E^*, cal/mole	f_0, sec^{-1}	Reference
Synthetic quartz	5–80 × 10^6	20–80	1.2×10^{-6}	155		*Mason*, 1958
Al_2O_3	11	1670	2×10^{-3}	6×10^4	8×10^8	*Chang*, 1961
Al_2O_3	41	1800	5×10^{-4}	6×10^4	8×10^8	*Chang*, 1961
MgO	2.7×10^7	270	1.6×10^{-3}	3.4×10^3	1.5×10^{10}	*Chang*, 1961
MgO (Fe-doped)	2.7×10^7	250	1.0×10^{-3}	3.4×10^3	3×10^{10}	*Chang*, 1961

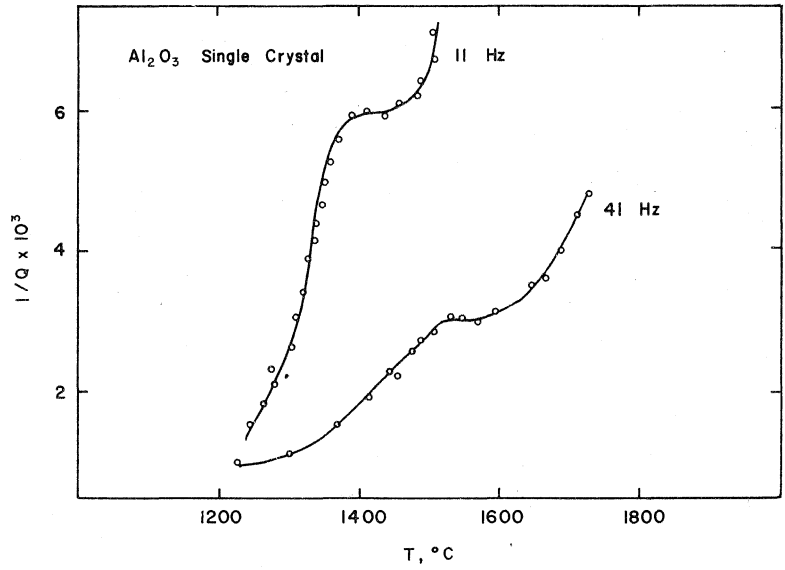

Fig. 8. Internal friction of single-crystal Al_2O_3 at high temperature, showing monotonic increase, with suspected Bordoni peak superimposed [*Chang*, 1961]. The melting temperature is 2050°C.

probably due to a dislocation mechanism, possibly to Bordoni relaxation. Their measurements were not carried to high enough temperature for any peak to be seen at such a high frequency, but they estimated an activation energy of 100 to 120 kcal/mole from the slope of a plot of Q^{-1} versus $1/T$. *Chang* [1961] found, from the shift of T_p with frequency, an activation energy of 60 kcal/mole. Moreover, an extrapolation of Chang's data to 50 kHz suggests that at this frequency the peak that Chang observed should occur at 4350°K, well past the melting point of Al_2O_3. Thus it seems unlikely that Chang observed the same phenomenon as Huber et al., and it is not known whether either phenomenon was the Bordoni relaxation.

RELAXATIONS CAUSED BY ATOMIC MOTIONS

There are many circumstances in which stress relaxation is caused by rearrangements of atoms into a position of lower Gibbs free energy in the stressed state. The atomic rearrangements may take place over quite large distances, as in the case of bulk atomic diffusion, or they may take place over some fraction of a lattice spacing, as in the case of an impurity jumping from one interstitial position to another. The relaxation time for these processes will be inversely proportional to the mobility of the appropriate atoms (and thus strongly temperature dependent), and, as in the case of thermoelastic diffusion, proportional to the square of the distance over which the atoms must travel. Thus, the relaxation time will be quite large for bulk diffusion due to a pressure gradient across, say, a grain diameter, and will be small for relaxation of an interstitial impurity into an adjacent, but lower energy, site.

Relaxation by Diffusion in a Stress-Wave-Induced Pressure or Temperature Gradient

If the solute atoms in a solid solution such as $(Mg,Fe)_2SiO_4$ or $(Mg,Fe)SiO_3$ are of larger size than the solvent atoms, they will tend to relieve compressional strain by diffusing into dilated regions. Conversely, small substitutional solute atoms and vacancies will diffuse toward regions of compression. As in the case of thermal diffusion, this mechanism operates principally for compressional waves, but would also cause attenuation of shear waves because of stress inhomogeneities. For longitudinal waves, the relaxation strength Δ is given by [*Bhatia*, 1967]

$$\Delta = \frac{M_U(\partial\epsilon/\partial x)^2}{(\partial^2 G/\partial x^2)} \tag{7}$$

where x is molar concentration of solute.
G is Gibbs free energy.
ϵ is longitudinal strain.
M_U is unrelaxed elastic modulus.

If the two components of this system are only partly miscible below some critical temperature T_c, and completely miscible above T_c, then a second-order phase transition occurs at T_c. The attenuation near the critical temperature of a second-order phase transition is discussed in a later section. For $| T - T_c | \gg 0$, it is usually true that $\Delta < 1$ [*Bhatia*, 1967]. In the case of an ideal solid solution, the factor $(\partial^2 G/\partial x^2)$ comes solely from the entropy of mixing

$$\partial^2 G/\partial x^2 = nkT/x(1 - x)$$

Putting this into equation 7, we get

$$\Delta = \frac{M_U - M_R}{M_U} = x(1 - x)\frac{WM_U}{\rho RT}\left(\frac{\partial\epsilon}{\partial x}\right)^2$$

where W is formula weight divided by number of available impurity sites per formula weight.
ρ is density.
$\partial\epsilon/\partial x \cong (a_2 - a_1)/a_1$, where a_1 is atomic radius of solvent, and a_2 is atomic radius of solute.

For forsterite with a 10% Fe/Mg ratio, and taking $W = 70$, $\rho = 3.3$ grams/cm^3, $M_U = 2 \times 10^{12}$ dynes/cm^2, and $(a_2 - a_1)/a_1 = (0.80 - 0.65)/0.65 = 0.23$, we get $\Delta \cong 1$ at 2000°K. Thus, if the relaxation time for this mechanism were in the range of seismic frequencies, this could be an important mechanism indeed. The relaxation time is given by

$$\tau = (d/a)^2(hN/H^*)\exp(H^*/RT)$$

where d is relaxation distance.
a is distance an atom moves in elementary diffusion.
h is Planck's constant.
N is Avogadro's number.
H^* is activation energy for diffusion.

Reasonable values for the activation energy range from 10 to more than 100 kcal/mole.

To evaluate the seismic significance of this mechanism, we compute the relaxation distance for which the relaxation time would equal 100 sec, assuming a temperature of 2000°K and a range of activation energy. Values are given in Table 7. Assuming that the relaxation distance in the mantle is approximately the grain diameter, an unreasonably small grain size would be required in the mantle for this mechanism to be important in attenuating seismic waves. Moreover, this type of relaxation has never been clearly identified in an oxide or silicate, although there is little work on silicate or oxide solid solutions.

Atomic Relaxation

There are many situations in which the nonequilibrium arrangement of the atoms induced by the applied stress is such that relaxation requires diffusion of atoms over only a few interatomic distances.

Point defects in solids may create asymmetry in a crystal lattice under stress, causing diffusion of atoms to positions of lower energy, relief of part of the stress, and, hence, internal friction. Examples of point defects are vacancies, substitutional impurities, interestitial impurities, and split (or 'dumbbell') self interstitials, in which two atoms occupy interstitial positions about an empty lattice site. Solute atoms in a dilute solid solution may be considered impurities. In ionic crystals, these various types of defects tend to exist in such combinations as to preserve charge neutrality. *Berry* [1962] has shown that isolated point defects may cause internal friction whenever the existence of the point defect causes a distortion that has a lower symmetry than that of the lattice. In a state of zero stress, an isolated point defect may occupy any of several crystallographically equivalent positions, all equal in energy. However, if the defect has the asymmetry described above, an applied stress will remove the degeneracy of the energy states, and the defects will prefer some sites over others. The asymmetry required would be expected only from interstitials, and only in certain lattices (e.g., interstitials occupying octahedral sites in a body-centered-cubic lattice). However, when the defect concentration becomes high enough that the defects are no longer effectively isolated, combinations of defects (of any kind) may have the asymmetry needed to remove the degeneracy of energy levels, and thus cause stress relaxation. The effect may be strongest

TABLE 7. Diffusion Relaxation Distance in the Mantle such that $\tau = 100$ sec*

Activation Energy, kcal/mole	Relaxation Distance, cm
10	2.2×10^{-4}
20	8.8×10^{-5}
40	1.0×10^{-5}
60	1.0×10^{-6}

* The values of d would be decreased by a factor of 10 for $\tau = 1$ sec.

in either compressional, longitudinal, or shear modes, depending on the symmetries of the crystal lattice and the lattice of available impurity sites.

The relaxation time for such a process is given by equation 3:

$$\tau = \tau_0 \exp (G^*/RT) = \tau_0 \exp (- S^*/R) \exp (H^*/RT)$$

Here τ_0 is approximately the period of the fundamental thermal vibrations, usually in the neighborhood of 10^{-12} to 10^{-13} sec. S^* is the entropy difference between the activated and original states of the jumping atom, and H^* is the height of the energy barrier. If S^* is large and negative, (i.e., the jump is a rather unlikely one, or requires an unlikely coincidence of events), the relaxation time may be rather long. However, the S^* term will usually be of little consequence, and the relaxation effect will show up only in very-high-frequency measurements.

The best known example of a short-range atomic relaxation effect occurs in the body-centered-cubic iron containing a small amount of nitrogen or carbon atoms (see, for example, *Snoek* [1941] and *Zener* [1948]). The nitrogen or carbon atoms dissolved in the iron occupy interstitial positions that are crystallographically equivalent in the absence of stress. When the lattice is compressed nonhydrostatically, some sites become more favorable than others and the crystal will attempt to maintain an equilibrium distribution, giving rise to an internal friction which is a maximum when the period of vibration is comparable with the relaxation time for the establishment of equilibrium. This effect has also been observed in α brass, which is a substitutional alloy with a face-centered-cubic structure in which zinc is dissolved in copper. The activation energy measured anelastically agrees with the activation energy for diffusion of zinc in copper.

A more detailed treatment of the conditions under which point defects cause internal friction in metals, as well as a review of pertinent data, has been given by *Berry* [1962], and a treatment of the internal friction from isolated point defects in oxide crystals appears in a work by *Wachtman et al.*, [1963]. What is important here is that each of the point defects may cause relaxation-type internal friction. The internal friction will increase with the point defect concentration, and maximum internal friction will occur when the frequency of the applied stress wave is equal to the 'jump frequency' of the pertinent atomic motion. This atomic jumping is thermally activated, so that $f_p = f_0 \exp (-H^*/RT)$, where H^* can be interpreted as the depth of the potential well out of which the diffusing atom must jump. H^* should also equal the activation energy for steady-state diffusion, and thus when the point defect causing a particular internal friction peak is known, the shift in the peak frequency with temperature should in principle give the activation energy of diffusion for the given point defect. The jump frequency depends on the material, the type of point defect (or combination of point defects), and of course the temperature. It may also be altered by the presence of dislocations and grain boundaries (which introduce local stress perturbations).

Relaxation effects also occur when an applied stress removes a degeneracy in order-disorder or twin-detwin pairs, and in general whenever atomic motions

act to lower the stored elastic energy of a solid body under applied stress. Again, the amount of the internal friction and the jump time vary widely.

Other examples of processes in which relaxation occurs by diffusion of atoms over only a few interatomic distances are:

Relaxation by diffusion of point defects in the local stress field of a dislocation, which might involve bulk diffusion of solute atoms, but would have a much shorter relaxation time than bulk diffusion across the grains because the relaxation distance may be only a few lattice spacings, and because diffusion might be strongly enhanced by the strong stress gradient around a dislocation. Such a process may contribute to relaxations that have been observed in oxides (data for which are shown below), although the causes of these relaxations are not known with certainty. This mechanism could affect both compressional and shear waves.

Twin-twin relaxations, in which stress may remove the degeneracy between the left- and right-hand configurations in a crystalline solid whose symmetry allows twinning. This effect has been observed in quartz at 36 kHz and 575°K [*Fraser,* 1964]. The relaxation time is far shorter than seismic periods even at room temperature, and at mantle temperatures would be shorter yet. This mechanism would apply primarily to shear waves.

Relaxations in Systems Undergoing Phase Transformations

In systems that are subject to solid-liquid or solid-solid phase transitions, small stresses can induce a reaction from one phase to another, causing stress relaxation. For two phases in equilibrium, the attenuation will be given by the standard relaxation formula

$$Q^{-1} = \Delta \frac{f/f_p}{1 + (f/f_p)^2}$$

where the relaxation strength Δ is given by [*Vaišnys,* 1968]

$$\Delta = [(C_\infty^2 - C_0^2)/C_0^2](V/C_0)$$

Here C is the complex phase velocity, and V is its real part. C_∞ and C_0 are the unrelaxed (high-frequency) and relaxed (zero-frequency) values of C, both of which are real. Δ is evaluated from the thermodynamic properties of the system by using

$$C^2 = (\partial p/\partial \rho)_s = \frac{-\gamma V}{\rho(\partial V/\partial p)_T}$$

where V is the molar volume and γ is the ratio of specific heats:

$$\gamma = C_P/C_0 = \frac{C_P}{C_P + T(\partial V/\partial T)_P^2/(\partial V/\partial P)_T}$$

This theory holds when both phases are present and in equilibrium. At the temperature of onset of a phase change, discontinuous volume changes occur that require a modified analysis. For most solid-liquid transitions, and for solid-solid transitions of geophysical interest, the relaxation strength will be large, of the order of magnitude 10^{-1} to 1 [*Vaišnys,* 1968]. The peak frequency will be determined by the kinetics of the appropriate reaction.

In the case of partial melting, the rate of liquid formation is given by

$$\dot{n}_{2l} = \sigma A\left(k_s - k_l \cdot \frac{n_{2l}}{n_{1l} + n_{2l}}\right)$$

where σA is the fraction of atoms in the interface region where they can react, k_s and k_l are rate constants for the solid-liquid and liquid-solid reactions, and where we have assumed a system of molar composition n_{1l}, n_{2l}, and n_{2s}; l and s denote liquid and solid, and the liquid is assumed to behave as an ideal solution. At equilibrium, $\dot{n}_{2l} = 0$, so that $k_s/k_l = n_{2l}{}^0/n_{1l} + n_{2l}{}^0$. Then for small deviations from equilibrium,

$$\Delta\dot{n}_{2l} = -k_l\sigma A n_{1l}/(n_{1l} + n_{2l}{}^0)^2\Delta n$$

where the superscript zero denotes an equilibrium value, and $\Delta n_{2l} = n_{2l} - n_{2l}{}^0$. Thus we have

$$f_p = \frac{1}{2\pi\tau} = \frac{k_l\sigma A}{2\pi} n_{1l}/(n_{1l} + n_{2l})^2$$

Usually, k_l can be described by an activation equation

$$k_l = \gamma_0 \exp\left[-(E^* + PV^*)/RT\right]$$

where γ_0 is some characteristic vibration frequency for the liquid. We then have

$$f_p = \frac{\gamma_0}{2\pi} \exp\left[-(E^* + PV^*)/RT\right]\sigma A n_{1l}/(n_{1l} + n_{2l})^2$$

This number depends strongly on parameters that are difficult to predict: σA, the fraction of molecules at the interface, will depend on the domain size and could vary by several orders of magnitude. Using $\gamma_0 = 10^{13}$ Hz, $\sigma A = 3 \times 10^{-7}$ $n_{1l} = n_{2l} = 0.01$, and an activation parameter appropriate to self diffusion in liquids, *Vaišnys* [1968] estimates that f_p might be in the seismic frequency band at some depth in the mantle.

It should also be mentioned that in addition to the chemical effect, partial melting can cause attenuation by scattering and by the mechanical coupling between the elastic solid and viscous liquid. We shall ignore the scattering effect because the dimension of any pocket of melt in the mantle is expected to be much smaller than a seismic wavelength. The internal friction caused by mechanical effects of partial melting will be discussed below in the section 'Viscous Mechanisms.'

In a pure melt, the net rate of liquid formation is given by

$$\Delta\dot{n}_l = (k_s - k_l)\sigma A$$

and is zero at equilibrium. If

$$k_s = \gamma_0 \exp - F_s{}^*/RT$$

$$k_l = \gamma_0 \exp - F_l{}^*/RT$$

then $F_s{}^* = F_l{}^*$ at equilibrium. Expanding $F_s{}^*$ and $F_l{}^*$, we find that

$$F_l^* = F_0^* + (\partial F_l^*/\partial T)_p \, \Delta T + (\partial F_l^*/\partial P)_T \, \Delta P = F_0^* - S_l \, \Delta T + V_l^* \, \Delta P$$

$$F_s^* = F_0^* - S_s^* \, \Delta T + V_s^* \, \Delta P$$

also $V_s^* - V_l^* = \Delta V_m$, the volume increase on melting, and $S_s^* - S_l^* = \Delta S_m$, the entropy of fusion. These relations lead to

$$d\Delta n_l/dt = -\sigma A[-\Delta V_m \Delta P + (\Delta H_m/T_0)\Delta T]/RT_0$$

The ΔT has two causes, adiabatic compression and the heat of reaction:

$$\Delta T = [T(\partial V/\partial T)_p/C_p]\Delta P - \Delta H_m \Delta n_l/C_{loc}$$

C_{loc} is the effective heat capacity at the reaction site, approximated by $C_p^\infty \delta A/V_m$, where C_p^∞ is the unrelaxed specific heat at constant pressure, A_t is the effective thermal interface area, δ is the depth to which the thermal wave penetrates, and V_m is the molar volume. The peak frequency is then given as [*Vaišnys*, 1968]

$$f_p = \frac{\gamma_0}{2\pi} \exp\,[-(E_l^* + PU_l^*)/RT]\sigma A(\Delta H_m)^2(V_m/\delta A_t)/C_p RT^2 \qquad (8)$$

This could be in the seismic bandwidth for mantle conditions.

The above arguments apply also to solid-solid transitions, with the difference that the activation parameters will be somewhat higher in solids. Other things being equal, this would imply longer relaxation times for the solid-solid transitions, but compensating effects might exist. In the solid transitions, cooperative phenomena may occur that overcome the high activation energy; *e.g.*, a local change in crystal structure will cause local stresses, which can act to encourage the phase change to propagate. Moreover, the rate constant k_l may contain pre-exponential factors indicating an inhibition not present in solids. An example of such an inhibition is the tendency of many melts to form 'anti-crystalline' clusters of a few hundred atoms on cooling toward the melting point [*Ubbelohde*, 1965]. Such clusters have a lower enthalpy than the melt, yet because of geometrical considerations are inconsistent with the crystal structure of the solid. Such effects might cause the liquid-solid reaction to be slower, not faster, than solid-solid reactions, and thus any comparisons of relaxation times based only on activation parameters should be regarded as speculative.

Attenuation at the Temperature of Onset of a Phase Change

At eutectic points, melting points of pure substances, and polymorphic phase transitions, discontinuous volume changes necessitate amendments to the above relaxation theory. The relaxation strength Δ has not been calculated for such cases, but it would presumably often be quite large (i.e., $\Delta \geq 1$). As can be seen from equation 8, at temperatures well above and below the transition temperature, where only one phase exists, the factor σA vanishes, so that $f_p = 0$ and $Q^{-1} = 0$. At the transition temperature itself, the two phases can be expected to be in contact over large areas, so that σA is large and f_p increases radically, by several orders of magnitude. If the experimental frequency f is in the range of values swept by f_p, we should expect a sharp peak in Q^{-1} at the transition tem-

perature. This effect has been observed in ice at its melting point [*Spetzler and Anderson,* 1968] and in quartz-bearing rocks at 3 kHz and 850°K [*Volarovitch and Gurvitch,* 1957], at which temperature a polymorphic transition occurs in quartz.

Attenuation near the Critical Temperature of a Second-Order Phase Transition

Many solids that are subject to second-order phase transitions exhibit a very sharp increase in attenuation when the temperature approaches T_c, the critical temperature. The thermodynamic state of such a system is dependent upon at least three independent variables. In the case where three are sufficient, we shall for convenience take the first two to be temperature and pressure, and for the third we shall use the variable ξ. For the example of an order-disorder transformation in an alloy, ξ would represent the order parameter. For $T \neq T_c$, the free energy G will depend on T, P, and ξ; we write $G = -S\delta T + V\delta P + z\delta\xi$. The condition for equilibrium is then

$$(\partial G/\partial \xi)_{P,T} = z(P, T, \xi) = 0$$

Because G must be independent of ξ at the critical point, we also have

$$(\partial^2 G/\partial \xi^2)_{P,T=T_c} = 0$$

and similarly for all higher-order derivatives.

However, the relaxation time is inversely proportional to the ordering force, $\varphi = (\partial z/\partial \xi)_{P,T} = (\partial^2 G/\partial \xi^2)_{P,T}$. Thus at the critical temperature, where the ordering force vanishes, the relaxation time becomes infinite. Similarly, the relaxation strength, $(M_U - M_R)/M_U$, drops discontinuously from some finite value to zero at the critical temperature. We thus expect a very sharp peak in attenuation just below the critical temperature where the relaxation time equals the period of vibration and the relaxation strength is still finite. As the temperature is increased, this peak is followed by a rapid drop in attenuation because the relaxation time exceeds the vibration period, and we expect no attenuation from this mechanism at the critical temperature itself.

Because it is seldom possible to determine the precise mechanism responsible for a relaxation peak, and because we wish to see if *any* of the atomic relaxations are likely to be important, we have assembled in Table 8 data from all the potentially important relaxation mechanisms observed in single crystals. We have included high-temperature data for oxide single crystals, but have not attempted to present data for metals or for any material at low temperature and high frequency.

The importance of these relaxations in the attenuation of seismic waves depends on the variation of the peak frequency with temperature and pressure, given by equation 5. Unless the peak frequency f_p under mantle conditions is near the range of seismic frequencies, the mechanism will not be important for seismic-wave attenuation. A convenient way to display the variation of f_p with temperature is to plot log f_p versus inverse temperature, as in Figure 5. Measurement of f_p for a single relaxation mechanism at two different temperatures determines two points on this plot, and a straight line through these points can

TABLE 8. Relaxation Peaks in Single-Crystal Oxides and Silicates

Sample	Impurities	f, Hz	Mode	T_{peak}, °K	Range T, °K	$(Q^{-1})_{peak}$	E^*, kcal/mole	$\tau_0 \exp(-S^*/R)$	Ref.	Remarks
Al_2O_3		7	Flex.	1370	300–1470	6×10^{-3}	200	2×10^{-34}	1	*a*
Al_2O_3		11	Flex.	1675	1520–1780	2×10^{-3}	64	6×10^{-11}	2	*a*
Al_2O_3		41	Flex.	1800	1510–2000	1×10^{-3}	64		2	*a*
Al_2O_3		23	Tors.	No peak found 300–1870°K					3	*b*
MgO		4.3×10^4	Long. and flex.	480	300–1100	3×10^{-5}	15	6×10^{-13}	4	*b*
MgO	Cr, Fe	3.8×10^4	Long. and flex.	1195	300–1400	4.3×10^{-5}	48	5×10^{-16}	5	*c*
TiO_2		2.70		330	300–400	2×10^{-3}	24	8×10^{-18}	6	*d*
MgO		1.7×10^5	Long. and flex.	537			15	6×10^{-13}	5	
Quartz		2.1×10^4	Long.			2.7×10^{-4}			7	*e*
Quartz		2.1×10^4	Long.	500	475–710	4.8×10^{-5}	27	1.7×10^{-17}	8	
Quartz		2.1×10^4	Long.	545	475–710	5.4×10^{-5}	13	7×10^{-11}	8	
Quartz		3.6×10^4	Tors.	550	300–830	8.3×10^{-4}	17	10^{-12}	9	*f*
Quartz		3.6×10^4	Long.	575	300–830	4.5×10^{-5}	22	2×10^{-14}	9	*g*
Quartz		5.1×10^4	Long.	596	300–830	2.1×10^{-5}	24	6×10^{-15}	7	
Quartz		5×10^6	Shear	50		2×10^{-6}			10	
Quartz	Li	5×10^6	Shear	50		2×10^{-6}	2.5	10^{-12}	10	
Quartz	Na	5×10^6	Shear	50		7×10^{-4}	1.6	10^{-12}	10	
Quartz	Na	5×10^6	Shear	140		3×10^{-6}	2.3	10^{-12}	10	
Quartz	K	5×10^6	Shear	210		10^{-5}	4.4	10^{-12}	10	

References

1. *Chang*, 1959
2. *Chang*, 1961
3. *Turnbaugh*, 1962
4. *Southgate*, 1965
5. *Southgate*, 1966
6. *Carnahan and Brittain*, 1963
7. *Wasilik*, 1957
8. *Alers*, 1964
9. *Cook and Breckenridge*, 1953
10. *Fraser*, 1964

Remarks

a. Deformed sample. Peak interpreted as Bordoni relaxation. E^* computed with aid of data from *Wachtman* [1957] on polycrystalline Al_2O_3. Value of E^* probably in error, resulting in unreasonable value for τ_0.

b. Q^{-1} about 3×10^{-3} for all temperatures 300–1870°K.

c. $(Q^{-1})_{peak}$ proportional to impurity concentration.

d. Peak interpreted as relaxation of Ti interstitial impurity.

e. $(Q^{-1})_{peak}$ increasing function of frequency.

f. $(Q^{-1})_{peak}$ independent of frequency for 3 harmonics.

g. Peak interpreted as twin-detwin relaxation.

be used to determine f_p at other temperatures (but at the same pressure). Such plots for the highest-temperature relaxations found in oxides and silicates are shown in Figure 9. The horizontal bars indicate measurements made at a single frequency over a range of temperatures, the highest temperature being given by the left end point of the bar. The dots represent internal friction peaks, and the sloping lines are each drawn through two peaks presumably caused by the same relaxation mechanism in the same material. One of the experimental points for MgO is off scale and is not shown in the diagram. The sloping line through the Al_2O_3 points indicates the alleged Bordoni relaxation found by *Chang* [1961] in deformed crystals only, and is not found at the appropriate temperature in an undeformed crystal; this is indicated by the horizontal bar labeled with reference 5 and the notation 'no peak.'

The approximate range of frequency and temperature sampled by surface waves in the mantle is indicated in the lower left corner of Figure 9. Of all the relaxations ever discussed in single-crystal silicates and oxides, only one projects into the area of seismic interest, and this is the relaxation found by *Chang* [1961] in deformed Al_2O_3. Although it is true that the effect of pressure is to increase the enthalpies of activation of atomic processes, retard the atomic motions, and thus drive the peak frequencies to lower values for a given temperature, the conclusion is inescapable that most of the relaxations so far observed in single crystals would not contribute to the damping of seismic waves in the mantle. In principal, there may be many atomic (or dislocation) relaxations in mantle-type crystals under mantle conditions. Complex motions involving the simultaneous movement of groups of atoms might have the long relaxation times required. The

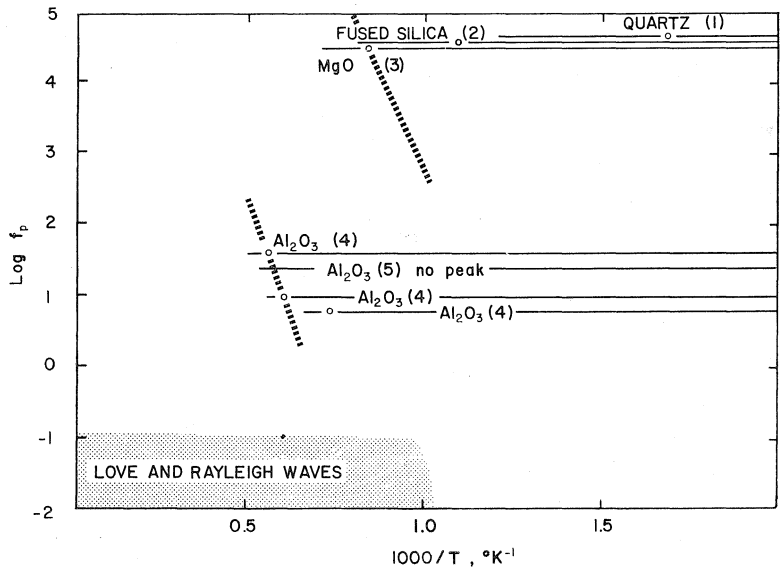

Fig. 9. High-temperature relaxation peaks in single crystals. Data from: (1) *Wasilik* [1957]; (2) *Marx and Sivertsen* [1953]; (3) *Southgate* [1966]; (4) *Chang* [1961]; (5) *Turnbaugh* [1962].

high-temperature, low-frequency measurements necessary to detect them have not yet been performed.

Grain Boundary Relaxations

In polycrystals, additional temperature-activated relaxations occur that are related to a stress relaxation mechanism at grain boundaries. In metals grain boundary relaxation peaks occur at temperatures of 300 to 1000°K, at frequencies near 1 Hz [*Kê,* 1947; *Leak,* 1962; *Pearson and Rotherham,* 1956]. For impure metals the activation energy is near that for self diffusion, but is reduced by a factor of ½ for very pure metals. In many very pure metals the activation energy for self diffusion near the grain boundaries is reduced by about half from that of self diffusion in the bulk, suggesting that the relaxation peak is connected with a stress-induced grain boundary diffusion [*Van Bueren,* 1961, p. 384].

Kê [1947] attempted to explain grain boundary relaxation by the presence of a viscous layer at the grain boundary. The stress relaxation time is $\eta D/Gd$, where η is the viscosity of the layer, D is the grain diameter, G is the unrelaxed shear modulus, and d is the thickness of the viscous layer. If $\eta = \eta_0 \exp(H^*/RT)$, where H^* is some activation enthalpy and η_0 is a constant,

$$f_p = \frac{1}{2\pi\tau} = \frac{Gd}{2\pi\eta_0 D} \exp(-H^*/RT) \tag{9}$$

for the frequency of maximum internal friction as a function of temperature. *Kê* [1949] assumed that the grain boundary was composed of regions of good grain-to-grain lattice fit, separated by regions of poor fit, and that deformation took place by forcing groups of atoms past one another in the regions of poor fit (his 'grain boundary slip' model). The activation energy should be that of volume self diffusion (i.e., the energy needed to distort the lattice enough to allow an atom to pass through) with no consideration being taken of the type or concentration of impurities at the boundary.

In a different model, *Mott* [1948] considered similar regions of good and bad fit, but assumed that deformation took place by actually removing atoms from the lattice in the regions of poor fit. The activation enthalpy would then be $H^* = nL(1 - T/T_m) \ln \sigma V/kT$, where n is the number of atoms that become separated, L is the latent heat of fusion for these atoms, T_m is the melting temperature, T the temperature, σ the applied stress, and V the molar volume. Mott's model may account for the effect of impurities, as L, T_m, and V will depend on the composition of the grain-boundary material.

Neither the Kê nor the Mott model has given a totally satisfactory quantitative explanation of the observed internal friction. Additional facts that need to be considered are the following:

1. Because of stress concentration near the grain boundaries, the grains themselves may actually deform by dislocation motion. Moreover, the dislocation density may be very high near the grain boundaries.
2. Impurities tend to collect at grain boundaries, and grain boundaries may act as either sources or sinks of point defects.

3. The energies needed to perform certain functions, such as unbinding an atom or distorting the lattice a certain amount, will be different at the grain boundaries from those in the interiors of grains. These energies depend on the type and concentration of impurities.
4. In a polymineralic aggregate, there is in general no lattice fit across grains and thus the 'good fit, bad fit' models are valid only in the sense that there is bad fit everywhere.

With the above remarks in mind, we consider the observations of grain-boundary relaxation in sintered oxides and rocks, treating the activation energy and the pre-exponential factor in equation 5 as empirically derived quantities. Table 9 gives the experimentally determined parameters for all observed thermally activated relaxations that occur in polycrystalline oxides and rocks at high temperatures which were found in the literature.

In Al_2O_3, peaks occur in doped samples that do not occur in pure samples. *Chang* [1959] found that in alumina doped with Cr_2O_3 the temperatures at which these peaks occur increase with increasing impurity concentration. Similar peaks were found in samples doped with SiO_2 and La_2O_3, but the peak temperatures decreased with increasing impurity concentrations. Measurements on highly pure samples of polycrystalline Al_2O_3 are in disagreement, as *Turnbaugh* [1962] failed to find a relaxation peak corresponding to that found by *Wachtman and Lam* [1958], *Chang* [1959], and *Chung et al.* [1962]. Some of the data for polycrystalline Al_2O_3 are shown in Figure 10, constructed in the same way as Figure 9. The open circles are relaxation peaks observed in nominally pure Al_2O_3; the crosses are peaks that occur in alumina doped with Cr_2O_3 but are absent in pure alumina. The horizontal bars on which no peaks are indicated represent measurements made by *Turnbaugh* [1962] on very pure Al_2O_3. It is seen that a high-temperature peak expected on the basis of the other observations on pure alumina is not present. Turnbaugh investigated the microstructure of all samples of pure Al_2O_3 used by the other investigators, and he concluded that those samples on which the peak was observed actually contained small amounts of a glassy phase at the grain boundaries. He found from his own internal friction measurements that the peak was present only in samples containing small amounts of alkalies and SiO_2 as impurities, which presumably precipitate at the grain boundaries to form the glassy phase. A further complication in the interpretation of this high-temperature peak is the observation by *Chang* [1959] that a similar effect also occurs in single-crystal Al_2O_3, (although to a smaller extent), as Figure 11 shows. This evidence implies that the high-temperature peak in Al_2O_3 is not caused by grain boundary viscosity as Kê and Mott believed, but by a more complex mechanism that involves dislocations as well as impurities.

In BeO, a 'pure' grain boundary peak occurs in addition to two lower temperature peaks associated with MgO impurity. These peaks are shown in Figure 12. Relaxation peaks occur in doped ZrO_2 as shown in Figure 13, but the data are not complete or consistent enough for activation energies to be inferred. No measurements have been reported for pure ZrO_2.

Because mantle materials are undoubtedly polycrystalline, at high temperature, and full of impurities (and/or separate phases at grain boundaries), it is

TABLE 9. Relaxation Peaks in Polycrystals

Sample	Impurities	f, Hz	Mode	T_{peak}, °K	Range T, °K	$(Q^{-1})_{peak}$	E^*, kcal/mole	$\tau_0 \exp(-S^*/R)$, sec	Ref.	Remarks
Al_2O_3	'Pure'	7	Flex.	1370	300–1450	4×10^{-2}	200	2×10^{-34}	1	*a, b*
Al_2O_3	1 wt % Cr_2O_3	5.7	Flex.	1130	300–1215	5×10^{-2}	47	2×10^{-11}	1	*a, c*
Al_2O_3	1 wt % Cr_2O_3	7	Flex.	1100	300–1470	2.5×10^{-2}			1	*a*
Al_2O_3	1 wt % Cr_2O_3	15.3	Flex.	1180	1020–1220	6.5×10^{-2}	47	2×10^{-11}	1	*a*
Al_2O_3	1 wt % Cr_2O_3	16	Flex.	1168					1	*a*
Al_2O_3	0.5 wt % Cr_2O_3	16	Flex.	1096					1	*a*
Al_2O_3	3 wt % Cr_2O_3	16	Flex.	1184					1	*d*
Al_2O_3	0.25 wt % La_2O_3	5.0	Flex.	1130	300–1230	3.5×10^{-2}			1	*a, e*
Al_2O_3	0.25% La_2O_3	15	Flex.	1150	300–1520	2.4×10^{-2}			1	*a*
Al_2O_3	0.25% La_2O_3	15	Flex.	1370	300–1520	2.2×10^{-2}			1	*a*
Al_2O_3	0.25% La_2O_3	15.7	Flex.	1170	1080–1260	3.5×10^{-2}			1	*a*
Al_2O_3	0.25 wt % La_2O_3	16	Flex.	1168					1	*a*
Al_2O_3	0.25 wt % La_2O_3	16	Flex.	1103					1	*a*
Al_2O_3	1 wt % La_2O_3	16	Flex.	1063					1	*a*
Al_2O_3	1 wt % Cr_2O_3	7	Flex.	1320	300–1470	2.5×10^{-2}			1	*a*
Al_2O_3	0.03–0.07 wt % carbon	5×10^3	Flex.	1350	300–1470	1.5×10^{-2}			2	*f*

TABLE 9 (*continued*)
Relaxation Peaks, Polycrystals

Sample	Impurities	f, Hz	Mode	T_{peak}, °K	Range T, °K	$(Q^{-1})_{peak}$	E^*, kcal/mole	$\tau_0 \exp(-S^*/R)$, sec	Ref.	Remarks
Al_2O_3	0.6 wt % SiO_2	5×10^3	Flex.	1364	300–1540	2.3×10^{-3}			2	*f, g*
Al_2O_3	0.6 wt % SiO_2	5×10^3	Flex.	995	300–1540	9×10^{-4}			2	*f, g*
Al_2O_3	1.0 wt % SiO_2	5×10^3	Flex.	1350	300–1470	2.2×10^{-1}			2	*h, g*
Al_2O_3	1.0 wt % SiO_2	5×10^3	Flex.	970	300–1470	6×10^{-1}			2	*h, g*
Al_2O_3	Pure	5×10^3		1488					3	
Al_2O_3	0.3–0.7 wt % carbon	5×10^3	Flex.	1350	300–1470	1.5×10^{-2}			4	
Al_2O_3	1 wt % SiO_2	1.5×10^4	Flex.	970	300–1470	6×10^{-3}			4	*f, g*
Al_2O_3	Porcelain	3.7	Flex.	1153	1070–1420	5×10^{-2}			5	*i*
Al_2O_3	SiO_2, alkalies	13	Flex.	1170	1075–1420	1.1×10^{-2}	35		5, 6	
Al_2O_3	SiO_2, alkalies	20	Flex.	1200	1075–1377	1.0×10^{-2}	35		5, 6	
Al_2O_3	MgO	23	Tors.		300–1260	No peak reported			7	*j*
Al_2O_3	Pure; no glassy phase	22	Tors.		300–1370	No peak reported			7	*j*
Al_2O_3	Pure; no glassy phase	22–26	Flex.		300–1765	No peak reported			5	*k, l*
Al_2O_3	1% Cr_2O_3	18–24	Flex.		300–1870	No peak reported			5	*k*
Al_2O_3	0.1% SiO_2	18–21	Flex.		876–1765	No peak reported			5	*m*
Al_2O_3	0.4% SiO_2	22–26	Flex.		1078–1748	No peak reported			5	*m*
Al_2O_3		1100	Flex.	1470	300–1500	3×10^{-2}	2×105	2×10^{-34}	8	*n*
Al_2O_3	15 wt % La_2O_3	2400	Flex.	480	300–1000	6×10^{-3}			9	

TABLE 9 (*continued*)
Relaxation Peaks, Polycrystals

Sample	Impurities	f, Hz	Mode	T_{peak}, °K	Range T, °K	$(Q^{-1})_{peak}$	E^*, kcal/mole	$\tau_0 \exp(-S^*/R)$, sec	Ref.	Remarks
Al_2O_3	Si, Mg, Ca, Na, L, 1%	2534	Flex.	1150	300–1330	3×10^{-3}			10	
BeO		5	Flex.	1630	1370–1670	7×10^{-2}	115	10^{-17}	1	*a, o*
BeO		30	Flex.	1730	970–1790	7×10^{-2}	115	10^{-17}	1	*a, o*
BeO	1% MgO	31	Flex.	1370	1220–1620	2.4×10^{-2}	35–40	2×10^{-9}	1	*a*
BeO	1% MgO	31	Flex.	1470	1220–1620	4.0×10^{-2}	35–40	5×10^{-9}	1	*a*
BeO	1% MgO	42	Flex.	1420	1270–1670	2×10^{-2}	35–40	2×10^{-9}	1	*a*
BeO	1% MgO	42	Flex.	1520	1220–1670	4×10^{-2}	35–40	5×10^{-9}	1	*a*
MgO	98% density	1400	Flex.		300–1570	No Peak			8	*p*
MgO		20	Tors.		300–1300	No Peak			7	*q*
ThO_2	1.5 mole % CaO; porosity, 1%	1390	Flex.	514		2×10^{-4}	21	2×10^{-13}	11	*r*
ZrO_2	13 mole % CaO	486	Flex.	560		2.2×10^{-2}	29	2×10^{-15}	12	*s*
ZrO_2	16 mole % CaO	582	Flex.	560		1.6×10^{-2}	43	4×10^{-21}	12	*s*
ZrO_2	10 mole % CaO	1250	Flex.	570		1×10^{-2}			9	
ZrO_2	10 mole % CaO	1250	Flex.	1130		1×10^{-2}			9	
ZrO_2	8 mole % CaO, 1.4% Al_2O_3	14	Tors.	470	300–1260	9×10^{-3}			7	*t*
ZrO_2	8 mole % CaO, 1.4% Al_2O_3	14	Tors.	750	300–1260	2×10^{-3}			7	*t*
ZrO_2	8 mole % CaO, 1.4% Al_2O_3	14	Tors.	1170	300–1260	1.3×10^{-3}			7	*t*

TABLE 9 (*continued*)
Relaxation Peaks, Polycrystals

Sample	Impurities	f, Hz	Mode	T_{peak}, °K	Range T, °K	$(Q^{-1})_{peak}$	E^*, kcal/mole	$\tau_0 \exp(-S^*/R)$, sec	Ref.	Remarks
Quartzite		3000	Shear	850	300–1270	7.8×10^{-3}			13	*u*
Sandstone		3000	Shear	850	300–1270	7.2×10^{-3}			13	*u*
Granite		3000	Shear	870	300–1170	3.6×10^{-3}			13	*u*
Diabase		3000	Shear	No peak	300–870				13	
Basalt		3000	Shear	No peak	300–1170				13	
Basalt glass		3000	Shear	No peak	300–970				13	
Diorite		3000		870	300–1170	2.8×10^{-3}			13	*u*
Labradorite		3000		870	300–1270	4×10^{-3}			13	*u*
Marble		3000			300–870	No Peak			13	
Limestone		3000			300–870	No Peak			13	

References

1. *Chang*, 1959
2. *Chung*, 1961
3. *Chung et al.*, 1962
4. *Crandall et al.*, 1961
5. *Turnbaugh*, 1962
6. *Turnbaugh and Norton*, 1968
7. *Dew*, 1950
8. *Wachtman and Maxwell*, 1957
9. *Wachtman et al.*, 1959
10. *Wachtman and Lam*, 1958
11. *Wachtman*, 1963
12. *Wachtman and Corwin*, 1965
13. *Volarovitch and Gurvitch*, 1957

Remarks

a. Grain size, 25–30 μ.
b. $(Q^{-1})_{peak} = 6 \times 10^{-3}$ in single crystal.
c. T_p increases with impurity concentration.
d. Grain size, 15μ.
e. T_p decreases with impurity concentration.
f. Grain size, 4μ.
g. Mullite formed between grains.
h. Grain size, 3μ.
i. Grain size, 5–15μ.
j. $(Q^{-1})_{max} = 7 \times 10^{-4}$.
k. Grain size, 40–60μ.
l. $(Q^{-1})_{max} = 1.6 \times 10^{-3}$.
m. Grain size, 1–5μ.
n. No peak appears in single crystal. In polycrystal, glassy phase found at grain boundaries. Sample is 93% theoret. density.
o. Same activation energy as vacancy diffusion.
p. 98% theoretical density.
q. Sample under shear stress of 18 bar.
r. Peak attributed to oxygen vacancy, calcium substitution defect pair.
s. Peak attributed to oxygen vacancy.
t. Sample under shear stress of 24 bar.
u. Peak attributed to quartz polymorphic transition at 850°K.

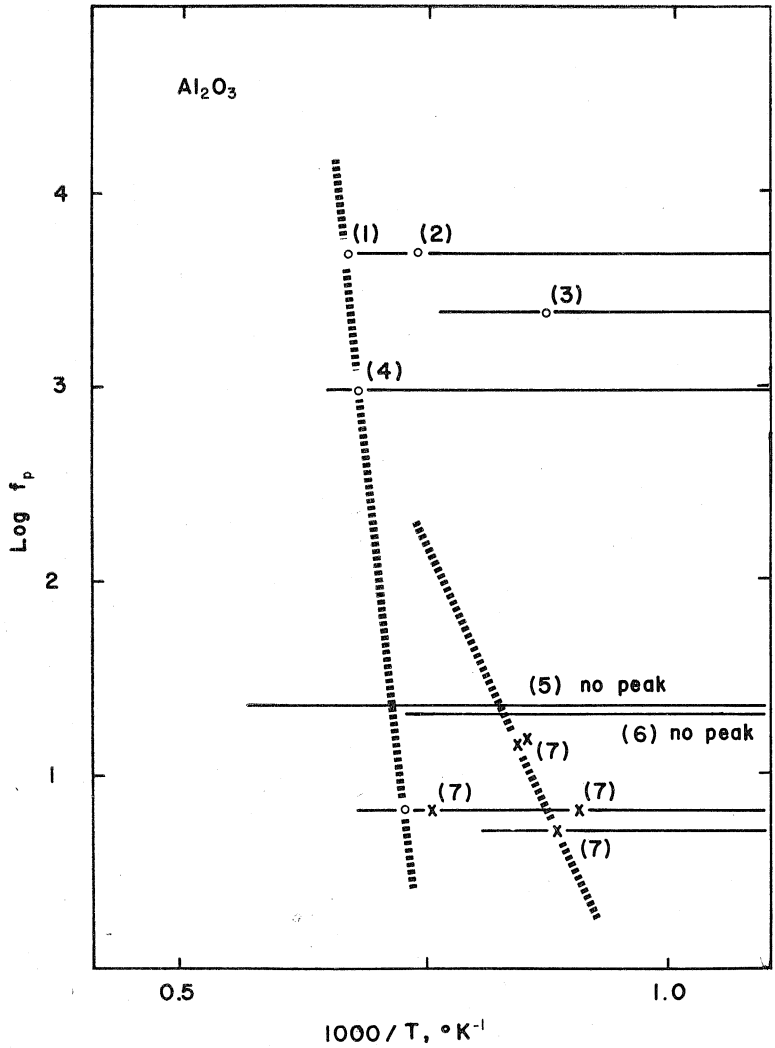

Fig. 10. High-temperature relaxation peaks in polycrystalline Al_2O_3. Data from: (1) *Chung et al.* [1962]; (2) *Chung* [1961]; (3) *Wachtman and Lam* [1958]; (4) *Wachtman and Maxwell* [1957]; (5) *Turnbaugh* [1962]; (6) *Dew* [1950]; (7) *Chang* [1959].

likely that the mechanisms responsible for the observed internal friction in polycrystalline ceramics may also cause seismic internal friction. Because the grain size and impurity content are likely to be important, and because different impurities may have quite different effects on the grain-boundary relaxation, a useful next step in an experimental program for geophysics would be to look for grain-boundary relaxations in possible mantle material, and to determine activation energies as in the oxides.

The effect of pressure on grain-boundary relaxation has not yet been studied for any material. Most probably, pressure would reduce the internal friction

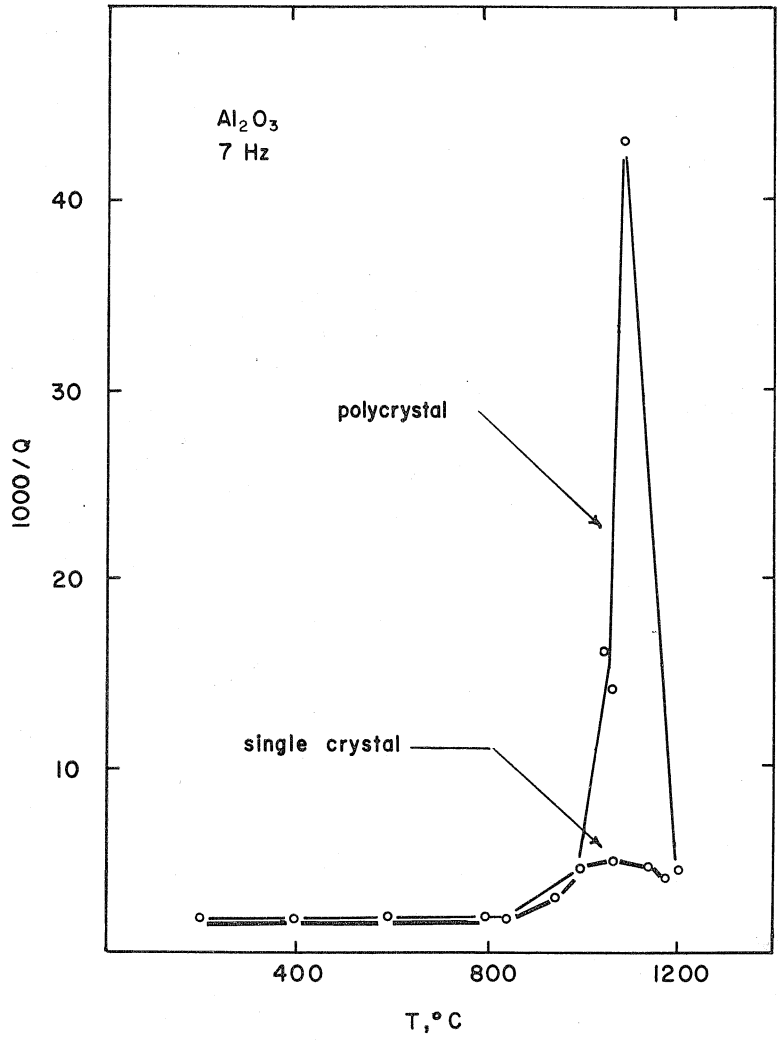

Fig. 11. Internal friction peaks in single-crystal and polycrystalline Al_2O_3 [*Chang*, 1959]. Note that $T(°K) < T_m$ (°K)/2.

peak and move it to a lower frequency for a given temperature, as pressure tends to impede atomic mobility.

Fitting of Seismic Data with Relaxation Mechanism

For a solid body with nonuniform elastic properties, the average attenuation will be given by

$$Q^{-1}(f) = \int_{\text{vol}} K(f, \mathbf{r}) Q^{-1}(f, \mathbf{r})\, d\mathbf{r}$$

where f is the frequency, $\mathbf{r}$ is the radius vector, $Q^{-1}(f, \mathbf{r})$ is the local intrinsic attenuation factor, and the kernel function $K(f, \mathbf{r})$ depends on the mode of wave propaga-

tion and the elastic properties of the solid body. For seismic surface waves, the kernel function represents the density of elastic energy stored by the seismic wave, and has been tabulated for several elastic models of the earth [e.g., *Anderson*, 1964].

Assuming a Q_β^{-1} of the form

$$Q_\beta^{-1}(f, \mathrm{r}) = \frac{M_U - M_R}{M_U} \frac{f/f_p(\mathrm{r})}{1 + [f/f_p(\mathrm{r})]^2}$$

where

$$f_p(\mathrm{r}) = f_0 \exp\{-[E^* + P(\mathrm{r})V^*]/RT(\mathrm{r})\}$$

and treating E^*, V^*, $(M_U - M_R)/M_U$, and f_0 as arbitrary parameters, constant for the whole earth, *Jackson* [1969] showed that the relaxation model could account for the observed attenuation of Love waves and torsional oscillations.

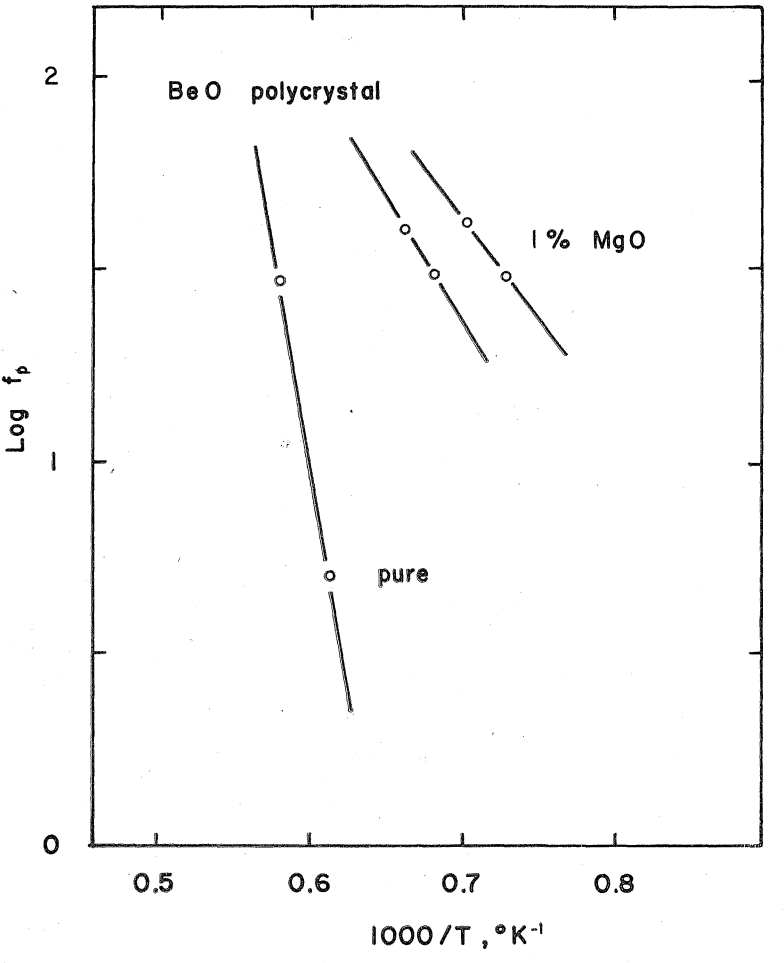

Fig. 12. High-temperature relaxation peaks in polycrystalline BeO. Data from *Chang* [1959].

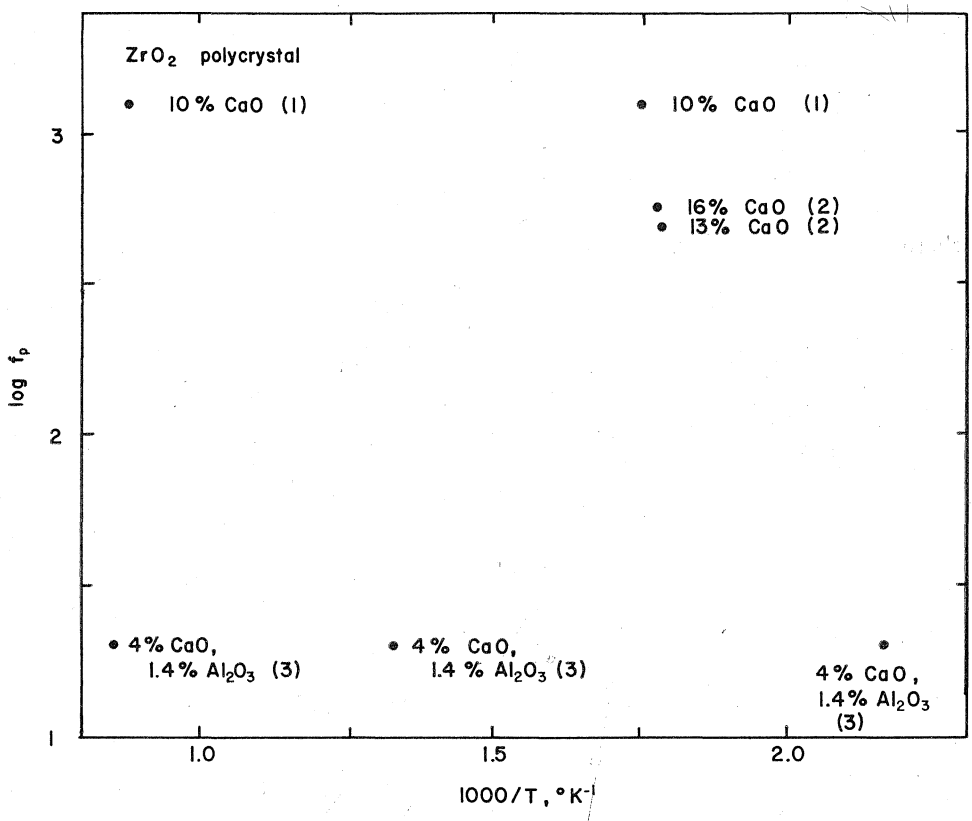

Fig. 13. High-temperature relaxation peaks in polycrystalline ZrO_2. Impurities in mole per cent. Data from: (1) *Wachtman et al.* [1959]; (2) *Wachtman and Corwin* [1965]; (3) *Dew* [1950].

These calculations made use of the kernel function for the CIT 13b oceanic earth model, the MacDonald 19b temperature model [*MacDonald,* 1959], and a pressure model by *Bullard* [1957]. Several sets of physically reasonable values for the four arbitrary constants gave a good fit to the seismic data. One of these models is compared with the seismic data in Figure 14.

The fact that this highly frequency-dependent model fits the data as well as previously frequency-independent models indicates that the presently available seismic data cannot answer the question of whether or not Q^{-1} has an intrinsic frequency dependence in the earth.

VISCOUS MECHANISMS

High-Temperature, Internal-Friction Background

The high-temperature internal friction of many materials can be represented by a series of peaks superimposed on a curve that increases monotonically with temperature. In the metallurgical literature this increase has been called the 'high-temperature, internal-friction background' and has been attributed to vacancy

creation and diffusion. This behavior occurs in both single crystals and polycrystals, although the internal friction in polycrystals is usually at least an order of magnitude greater than in single crystals, other conditions remaining the same. The internal friction is often an inverse function of the frequency and seems to obey a law of the form

$$Q^{-1} = (A/f) \exp(-H^*/RT) \tag{10}$$

where A is a constant and H^* is the activation energy for this mechanism. Both A and H^* will be functions of the concentration of impurities and other physical defects in the sample.

Some of the best data on internal friction in a solid near its melting point has been obtained for ice, both pure and doped [*Kuroiwa*, 1964]. These data are in good agreement with equation 10, as Figure 15 shows. A low-temperature relaxation peak has been subtracted from Kuroiwa's data before plotting this figure. The effect of impurities in the ice is to increase the internal friction at a given temperature, as shown in Figure 16. This effect could be caused by an

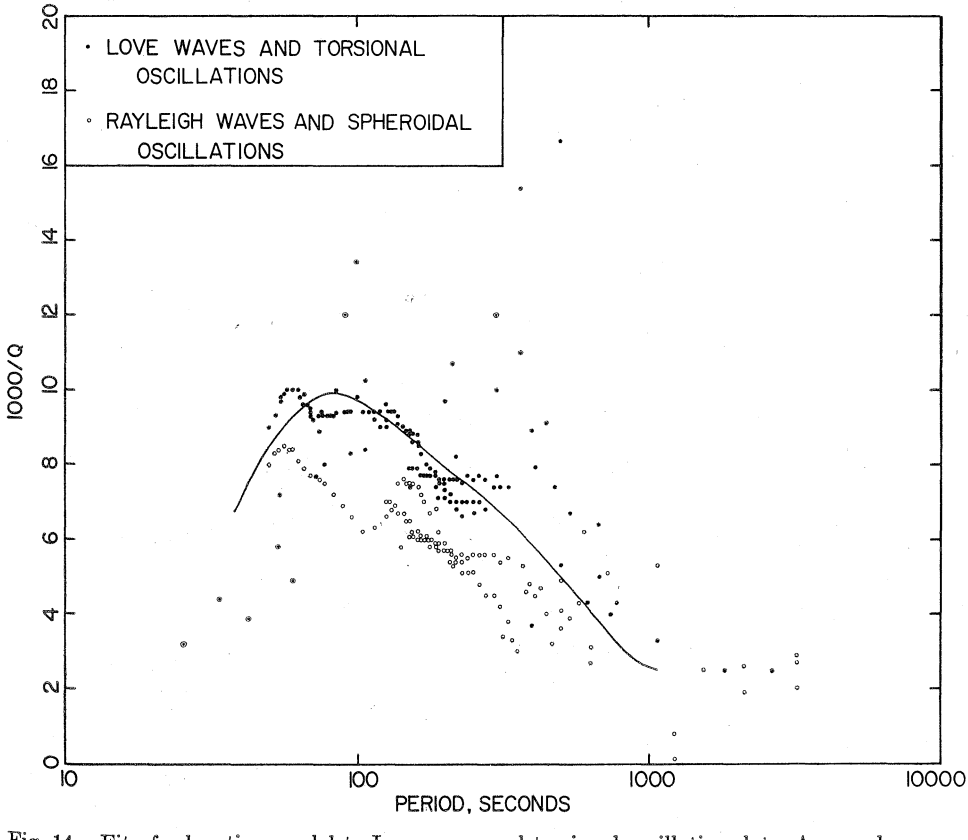

Fig. 14. Fit of relaxation model to Love-wave and torsional-oscillation data. Assumed parameters were $E^* = 80$ kcal/mole, $V^* = 4$ cm^3/mole, $f_0 = 10^{11}$ Hz, $(M_U - M_R)/M_U = 0.165$.

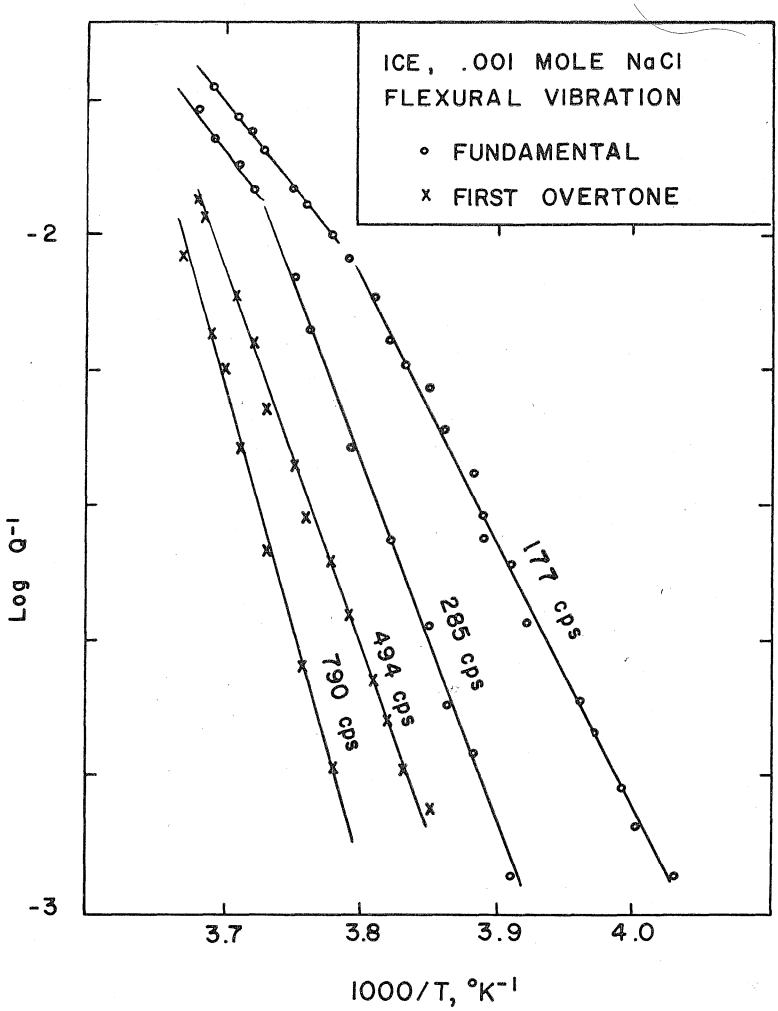

Fig. 15. Internal friction in doped polycrystalline ice near the melting point. Data from *Kuroiwa* [1964], with effects of a lower-temperature relaxation peak subtracted. The eutectic temperature of the NaCl-ice system corresponds to $1000/T$ of 3.98. As the temperature increases the amount of fluid phase increases. Most of the data on this figure are for the two-phase system ice-brine.

increase in the factor A of equation 10, a decrease in the activation energy, or both.

The anelastic behavior of polycrystalline Al_2O_3 near the melting point is similar to that of ice in that the internal friction is higher at every temperature in a doped specimen than in a similar pure specimen. This is demonstrated in Figure 17. Notice also that a relaxation peak occurs in the doped specimen but is absent in the pure specimen.

Internal-friction data for several oxides and silicates are shown in Figure 18. Notice that, at very high temperature, an order of magnitude change in Q^{-1}

can be caused by a 10 to 20% change in the absolute temperature. All samples are polycrystalline unless otherwise indicated. These data illustrate the properties mentioned above:

1. In all cases except the MgO at 3×10^4 Hz, the internal friction increases with temperature in approximate agreement with equation 10. In the exceptional case, the monotonic increase may be hidden by a relaxation peak. Also, the measurement was carried to only 0.4 of the melting point of MgO, so that the 'high temperature background' may occur at much higher temperatures.
2. The internal friction is an inverse function of the frequency. Compare Al_2O_3 at 13 Hz and 25 Hz, MgO single crystals at 3×10^4 Hz and 1.6×10^5 Hz.

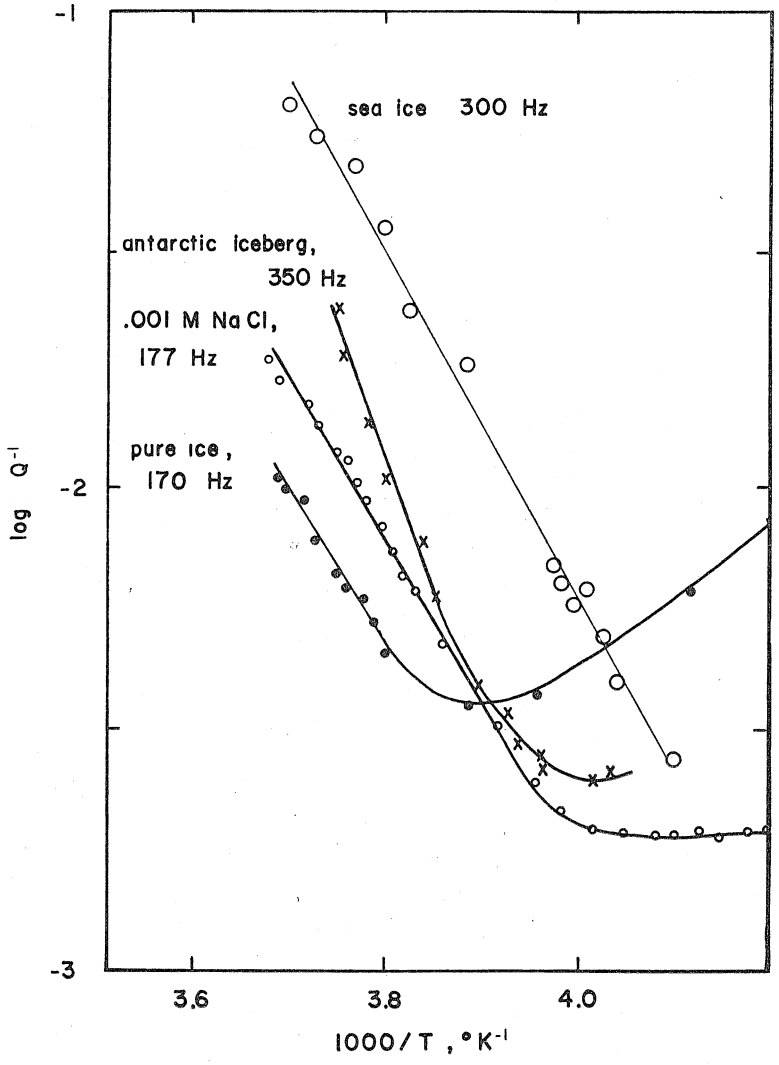

Fig. 16. Internal friction in polycrystalline ice near the melting point. Data for sea ice are from *Tabata* [1959], all other data are from *Kuroiwa* [1964].

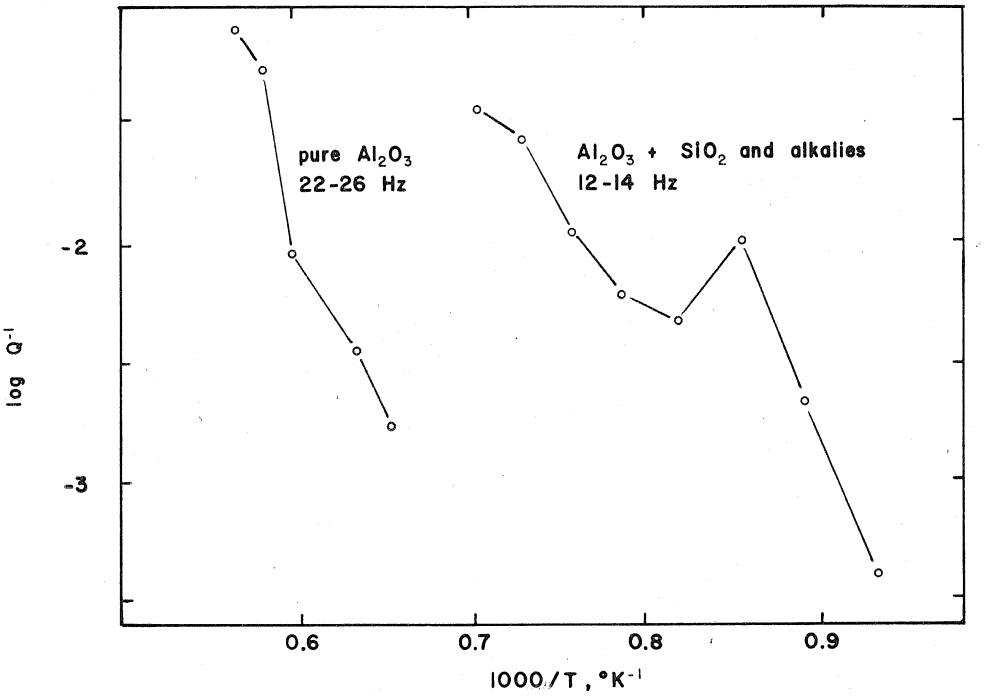

Fig. 17. High-temperature internal friction of Al_2O_3. Data from *Turnbaugh* [1962].

3. The internal friction in polycrystalline specimens is much higher than that in single crystals: compare polycrystalline Al_2O_3 at 13 Hz with single-crystal Al_2O_3 at 11 Hz. Moreover, the Al_2O_3 single crystals were deformed before testing to introduce dislocations. The internal friction in undeformed specimens was less than 2×10^{-5} at all temperatures up to 2070°K [*Chang*, 1959].

The frequency and temperature dependence of high-temperature internal-friction background can be explained in terms of the thermally activated relaxation mechanism. From equation 6, the internal friction for a relaxation mechanism is given by

$$Q^{-1} = \left[\frac{M_U - M_R}{M_U}\right] \frac{f/f_0 \exp(-H^*/RT)}{1 + [f/f_0 \exp(-H^*/RT)]^2}$$

If

$$f \gg f_p = f_0 \exp(-H^*/RT)$$

then

$$Q^{-1} = 2C \frac{f_0 \exp(-H^*/RT)}{f} \tag{11}$$

which is identical to equation 10, with $2Cf_0 = A$. At a given frequency, there exists a temperature $T_p = -H^*/(k \cdot \ln f/f_0)$ such that equation 6 has a maximum. If this temperature is greater than the melting point of the solid, then no maximum will be seen in the data, as equation 6 will not hold for the molten ma-

terial. However, T_p is still is a valid parameter for describing the internal friction below the melting point. Furthermore, if the high-temperature background is indeed caused by a relaxation phenomenon, one might expect that, at sufficiently low frequency, T_p would be less than the melting temperature, and a peak would be seen in a plot of internal friction versus temperature. The condition for this maximum to occur is

$$f < f_0 \exp [(- H^*)/RT_m] \tag{12}$$

where T_m is the melting temperature. The fact that no maximum has occurred in the internal friction of ice at 177 Hz (see Figure 15) allows the use of inequality 12 to obtain an upper limit for the quantity f_0 for the NaCl-doped ice examined by Kuroiwa:

$$f_0 < f \exp [(H^*)/RT_m] = 10^{15}\text{Hz} \tag{13}$$

The fact that the curve for ice at 177 Hz deviates negatively from a straight line implies that T_p at 177 Hz is only slightly greater than the final melting temperature of ice, and therefore that condition 12 is almost satisfied.

The fact that the internal friction increases rapidly in many solids near their melting points suggests that the mechanism responsible for the internal

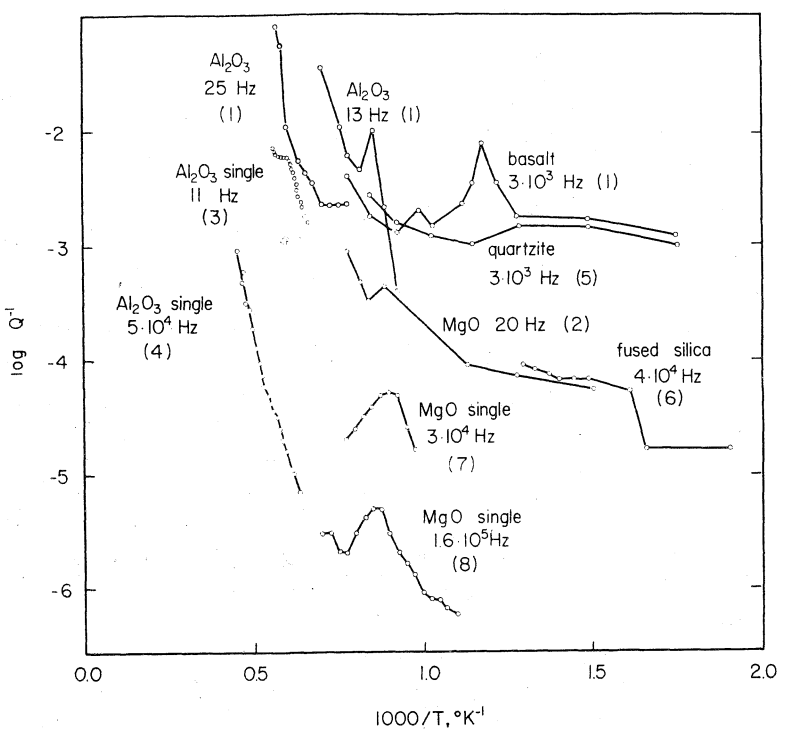

Fig. 18. High-temperature internal friction for several oxides and silicates. Data from: (1) *Turnbaugh* [1962]; (2) *Dew* [1950]; (3) *Chang* [1961]; (4) *Huber et. al.* [1961]; (5) *Volarovitch and Gurvitch* [1957]; (6) *Marx and Sivertsen* [1953].

friction is connected with the mechanism of melting. In fact, it has been suggested that melting might be a thermally activated phenomenon, as the high temperature background seems to be. *Nachtrieb* [1957] proposed that melting occurs when the density of mobile lattice vacancies reaches a critical value. The relative vacancy concentration is given by

$$c = \exp(-H^*/RT) \tag{14}$$

where H^* is the activation enthalpy for vacancy formation. Thus melting occurs when

$$c = c_m = \exp(-H^*/RT_m) \tag{15}$$

where c_m is the critical vacancy concentration for melting to occur. Thus the activation enthalpy for vacancy formation is related to the melting temperature by the equation

$$H^* = -RT_m \ln c_m \tag{16}$$

If the high-temperature background were controlled by the same mechanism, then

$$f_p = f_0 \exp(-H^*/RT) = f_0 \exp[(T_m/T) \ln c_m] \tag{17}$$

and for $f \gg f_p$,

$$Q^{-1} = \frac{M_U - M_R}{M_U} \frac{f_0}{f} \exp[(T_m/T) \ln c_m] \tag{18}$$

Equation 18 suggests that if the critical vacancy concentration is the same for all solids, a plot of $\ln Q^{-1}$ versus T_m/T for many different solids would yield a family of straight lines with the same slope. Such a plot is shown in Figure 19, and it is evident that the slopes of the curves are not the same. Thus either the mechanisms controlling melting and internal friction are not the same, or else the critical concentration of mobile vacancies varies considerably from one solid to another.

The high-temperature background is very similar, if not identical, to a phenomenon seen in metals and labeled 'high-temperature dislocation damping' [*Van Bueren*, 1961]. In a few metals (copper, aluminum) the activation energy for internal friction is approximately equal to that for vacancy diffusion, but for other metals, the activation energies are quite different. Possible explanations for the phenomenon include damped oscillation of dislocations in an internal stress field, impeded motion of dislocations through a field of point defects, and dislocations dragging point defects to which they are pinned. As for nonmetals, however, the experimental work has not been systematic enough to clearly identify the mechanism of stress relaxation.

In conclusion, it seems that the high-temperature, internal-friction background is caused by a thermally activated relaxation process. The presence of this effect in deformed Al_2O_3 single crystals, and its absence in similar but undeformed samples, indicate that dislocations are involved. The difference in internal friction between polycrystalline specimens and single crystals and the effect of impurities indicate that the mechanism responsible for the internal fric-

tion is strongly enhanced at grain boundaries, where the dislocation density is high and where impurity atoms may precipitate as a glassy phase.

Table 10 gives values of the important parameters of this high-temperature rise for the oxides, silicates, and glasses for which high-temperature data are available. Few experiments were complete enough to allow computation of activation energies, and it seems that no studies have been made to determine the effects of pressure or of grain size on the process involved. Isolating the mechanism of this high-temperature internal friction rise, and determining with much better accuracy the effects of temperature, pressure, frequency, and grain size are important experimental problems to be solved before the anelastic properties of the earth can be understood.

The high-temperature background attenuation is very strong at high temperatures in very pure materials. An order-of-magnitude increase in Q^{-1} can be obtained by raising the temperature some 200°C (see Figure 19). Unfortunately, experiments of this type have only been done at atmospheric pressure. Pressure undoubtedly suppresses this effect but possibly only to the extent that it raises the melting temperature. Although data are sparse, there is some suggestion (Figure 18) that the effect of temperature is not as pronounced on materials as chemically and geometrically complex as rocks. However, until measurements are made on pore- and crack-free rocks at relatively low frequencies and preferably at high pressure, it must be assumed that the large temperature effect measured on high quality oxides may occur in the mantle. The effect of one order of magnitude or less on attenuation that accompanies partial melting therefore is not yet a convincing argument in discussions of partial melting in the mantle. However, if it could be shown that the high attenuation zone of the upper mantle started and terminated abruptly rather than gradually, it would probably indicate partial melting.

An extensive experimental program on complex silicates at high temperatures and in the vicinity of the solidus performed at modest confining pressure and involving measurements of V_p, V_s, Q_p^{-1}, and Q_s^{-1} as a function of frequency and grain size is required in order to take full advantage of the seismic data.

INTERNAL FRICTION CAUSED BY MECHANICAL EFFECTS OF PARTIAL MELTING

Several seismic studies have indicated that increased absorption, particularly of S waves, occurs below volcanic zones and is therefore presumably related to partial melting. *Utsu* [1966] suggests that the Q^{-1} in the upper mantle in different regions in Japan varies by a factor of 10. Similar effects occur in the western United States [*McGinley and Anderson,* 1969]. Regional variations in seismic absorption may prove to be a powerful tool in mapping the thermal state of the upper mantle. Preliminary results indicate that, where the absorption is anomalously high, S is more affected than P. It has also been suggested that partial melting is the most probable cause of the low-velocity layer in the upper mantle of the earth [*Anderson and Sammis,* 1968]. Thus the role of partial melting in the attenuation of seismic waves may be a critical one, at least in certain regions of the earth.

TABLE 10. High-Temperature Background

Sample	Impurities	f, Hz	Mode	Range T, °K	Rise Begins, °K	$(Q^{-1})_{max}$	E^*, kcal/mole	A, sec^{-1}	Ref.	Remarks
				In Polycrystals						
Al_2O_3	'Pure'	7	Flex.	300–1450		No background rise			1	*a*
Al_2O_3	1 wt % Cr_2O_3	7	Flex.	300–1470	~1100	4×10^{-2}	17		1	*a*
Al_2O_3	0.25 wt % La_2O_3	15	Flex.	300–1475	~1100	6×10^{-2}	20		1	*a*
Al_2O_3	1% silica	1.5×10^4	Flex.	300–1470	~1100	5×10^{-3}	42		2	
Al_2O_3 porcelain		3.7	Flex.	1070–1420	~1270	6×10^{-2}	52		3, 4	
Al_2O_3		2534	Flex.	1070–1320	~1270	5×10^{-3}			5	
Al_2O_3	0.6% SiO_2	5×10^3	Flex.	300–1270	~1400	2.3×10^{-2}	51		6	*b*
Al_2O_3	Pure	22	Flex.	300–1765	~1478	8×10^{-2}	52		3, 4	*c*
Al_2O_3	1% Cr_2O_3	18	Flex.	300–1870	~1428	1.1×10^{-1}	52		3, 4	*c*
Al_2O_3	0.1% SiO_2	18	Flex.	876–1765	~1473	9×10^{-2}	52		3, 4	*d*
Al_2O_3	0.4% SiO_2	22	Flex.	1078–1748	~1463	8×10^{-2}	52		3, 4	*d*
Al_2O_3	SiO_2, alkalies glassy phase	12.6	Flex.	1073–1420	1223	4×10^{-2}	52		3, 4	*e*
Al_2O_3	SiO_2, alkalies glassy phase	19	Flex.	1073–1377		1.3×10^{-2}	52		3, 4	
Al_2O_3	SiO_2, alkalies glassy phase	11	Flex.	1071–1604	1397	3.9×10^{-2}	52		3, 4	*f*
Al_2O_3	Pure, no glassy phase	22	Tors.	300–1370	1070	$7 \times 10^{-4(?)}$			7	*g*
Al_2O_3	MgO	23	Tors.	300–1260	1250	$1.6 \times 10^{-3(?)}$			7	*h*
BeO	1% MgO	31	Flex.	1220–1670	1220	7×10^{-2}			1	*a*
BeO	1% MgO	42	Flex.	1220–1670	1220	7×10^{-2}			1	*a*
Al_2O_3	98% Al_2O_3 3.71 g/cm³ = 93%	2534	Flex.	300–1330		5×10^{-3}			5	
MgO	'Pure' 3.50 g/cm³	1400	Flex.	300–1570	1270	1.7×10^{-2}			8	
Al_2O_3	15 wt % La_2O_3	2400	Flex.	300–970	700	6×10^{-3}			9	
ZrO_2	5 wt % CaO	1250	Flex.	300–1520	1200	2.5×10^{-2}			9	
MgO	1% impurities	20	Tors.	300–1278	1000	9×10^{-4}			7	
ZrO_2		14	Tors.	300–1260		No background rise			7	*i*

TABLE 10 (*continued*)
High-Temperature Background

Sample	Impurities	f, Hz	Mode	Range T, °K	Rise Begins, °K	$(Q^{-1})_{max}$	E^*, kcal/mole	A, sec^{-1}	Ref.	Remarks
Ice	Pure commercial	170	Flex.	90–272		1×10^{-2}	17		10	*j*
Ice	Pure commercial	297	Flex.	90–272		6×10^{-3}	24		10	*j*
D_2O ice		116	Flex.	90–272		1.7×10^{-2}	17		10	*j*
Ice (0.001 mole NaCl)		177	Flex.	90–272		1.7×10^{-2}	13	7.9×10^{12}	10	*j*
Ice (0.001 mole NaCl)		285	Flex.	90–272		1.5×10^{-2}	13	1×10^{16}	10	*j*
Ice (0.001 mole NaCl)		494	Flex.	90–272		1.1×10^{-2}	16	1.6×10^{18}	10	*k*
Ice (0.001 mole NaCl)		790	Flex.	90–272		9×10^{-3}	16	7.1×10^{24}	10	*k*
Ice (0.002 mole HCl)		338	Flex.	90–272		1.6×10^{-2}	20	5×10^{14}	10	*j*
Ice (0.002 mole HCl)		940	Flex.	90–272		1.3×10^{-2}	24	2.5×10^{17}	10	*k*
Ice (0.002 mole NaOH)		270	Flex.	90–272		1.4×10^{-2}	27	6×10^{19}	10	*j*
Ice (0.002 mole NaOH)		750	Flex.	90–272		1.2×10^{-2}	41	1×10^{31}	10	*k*
Ice (0.005 mole HF)		340	Flex.	90–272		1.3×10^{-2}	23	2×10^{16}	10	*j*
Ice (0.005 mole HF)		930	Flex.	90–272		1.1×10^{-2}	33	6×10^{24}	10	*k*
Ice (0.01 mole NH_4F)		293	Flex.	90–272		1.6×10^{-2}	22	2.5×10^{16}	10	*j*
Ice (0.01 mole NH_4F)		805	Flex.	90–272		1.2×10^{-2}	34	4×10^{29}	10	*k*
Greenland ice		225	Flex.	90–272		1.5×10^{-2}	25	2×10^{19}	10	*j*
Greenland ice		492	Flex.	90–272		2.0×10^{-2}	25	8×10^{18}	10	*k*
Antarctic ice		370	Flex.	90–272		1.1×10^{-2}	26	3×10^{19}	10	*j*
Antarctic ice		350	Flex.	90–272		2.4×10^{-2}	27	6×10^{20}	10	*k*
LeConte glacier ice		260	Flex.	90–272		1.6×10^{-2}	27	5×10^{19}	10	
LeConte glacier ice		460	Flex.	90–272		9×10^{-3}	42	2×10^{32}	10	
LeConte glacier ice		718	Flex.	90–272		1×10^{-2}	36	2×10^{27}	10	
LeConte glacier ice		245	Flex.	90–272		2.5×10^{-2}	21	7×10^{15}	10	
LeConte glacier ice		430	Flex.	90–272		1.6×10^{-2}	29	4×10^{22}	10	
LeConte glacier ice		670	Flex.	90–272		1.2×10^{-2}	30	2×10^{23}	10	
Sea ice		~300	Flex.	243–270		8×10^{-2}	18	8×10^{13}	11	
Sea ice		~300	Flex.	251–270		9×10^{-2}	16	1.6×10^{12}	11	
Sea ice		~300	Flex.	252–270		5×10^{-2}	17	2.5×10^{12}	11	

TABLE 10 (*continued*)
High-Temperature Background

Sample	Impurities	f, Hz	Mode	Range T, °K	Rise Begins, °K	$(Q^{-1})_{max}$	E^*, kcal/mole	A, sec^{-1}	Ref.	Remarks
Sea ice		~300	Flex.	244–270		6×10^{-2}	18	2×10^{13}	11	
Sea ice		~300	Flex.	248–270		4×10^{-2}	14	2×10^{10}	11	
Sea ice		~300	Flex.	247–270		3.5×10^{-2}	15	2.5×10^{10}	11	
Granite		3000	Shear	300–1170		1.45×10^{-2}			12	
Diabase		3000	Shear	300–870		4.2×10^{-3}			12	
Basalt		3000	Shear	300–1170		3.5×10^{-3}			12	
Basalt glass		3000	Shear	300–1070		1.7×10^{-2}			12	
Gabbro		3000		300–850		7.5×10^{-3}			12	
Diorite		3000		300–1270		9.8×10^{-3}			12	
Labradorite		3000		300–1170		7×10^{-3}			12	
Marble		3000		300–870		6×10^{-3}			12	
Limestone		3000		300–870		3.3×10^{-3}			12	
Quartzite		3000		300–1270		4×10^{-3}			12	
Sandstone		3000		300–1270		8.7×10^{-3}			12	
				In Single Crystals						
Al_2O_3		11	Flex.	1450–1780	1450	7×10^{-3}	26.5–30	1.2×10^{1} 3.5×10^{1}	13	*m*
Al_2O_3		41	Flex.	1450–2000	1450	5×10^{-3}	$2–3 \times 10^{4}$	1.3	13	*m*
Al_2O_3		5×10^{4}		300–2050	1770	6×10^{-3} deformed, 10^{-5} undeformed	6.5×10^{4} 9.8×10^{4}	3×10^{3} 3×10^{7}	14	*n*
Al_2O_3		22		300–1840		4×10^{-3}	No background rise		3	*o*
Quartz	Undoped natural quartz	5×10^{6}	Flex.	Identical to Li-doped sample at 5 MHz					15	
Quartz	Li-doped natural quartz	3×10^{6}	Flex.	4–640		5×10^{-4}	17		15	*p*

TABLE 10 (*continued*)
High-Temperature Background

Sample	Impurities	f, Hz	Mode	Range T, °K	Rise Begins, °K	$(Q^{-1})_{max}$	E^* kcal/mole	A, sec^{-1}	Ref.	Remarks
Quartz	Li-doped natural quartz	5×10^6	Flex.	4–690		7×10^{-4}	17		15	*p*
Quartz	Li-doped natural quartz	9×10^6	Flex.	4–640		1.5×10^{-4}	17		15	*p*
Quartz	K-doped natural quartz	5×10^6	Flex.	4–820		1×10^{-3}	18		15	*q*
Quartz	Na-doped natural quartz	5×10^6	Flex.	4–830		4×10^{-4}	21		15	*r*
Quartz		5×10^4		300–830		1×10^{-4}	2.0	4.6×10^{15}	16	
Quartz		5×10^4		300–830		1×10^{-4}	26	2×10^2	16	

References

1. *Chang*, 1959
2. *Crandall et al.*, 1961
3. *Turnbaugh*, 1962
4. *Turnbaugh and Norton*, 1968
5. *Wachtman and Lam*, 1958
6. *Chung*, 1961
7. *Dew*, 1950
8. *Wachtman and Maxwell*, 1957
9. *Wachtman et al.*, 1959
10. *Kuroiwa*, 1964
11. *Tabata*, 1959
12. *Volarovitch and Gurvitch*, 1957
13. *Chang*, 1961
14. *Huber et al.*, 1961
15. *Fraser*, 1964
16. *Wasilik*, 1957

Remarks

a. Grain size, 25–30μ.
b. Grain size, 4μ.
c. Grain size, 40–60μ.
d. Grain size, 1–5μ.
e. Grain size, 5–10μ.
f. Grain size, 5–15μ.
g. Sample under shear stress of 21 bars.
h. Sample under shear stress of 6 bars.
i. $Q^{-1} = 4 \times 10^{-4}$ at 1260°K.
j. Fundamental flexural mode.
k. First overtone flexural mode.
l. Background may be edge of 850° peak.
m. Sample deformed before testing.
n. Q^{-1} strongly dependent on dislocation density.
o. $Q^{-1} = 4 \times 10^{-3}$ at 300°K.
p. Same activation energy as lithium diffusion.
q. Same activation energy as potassium diffusion.
r. Same activation energy as sodium diffusion.

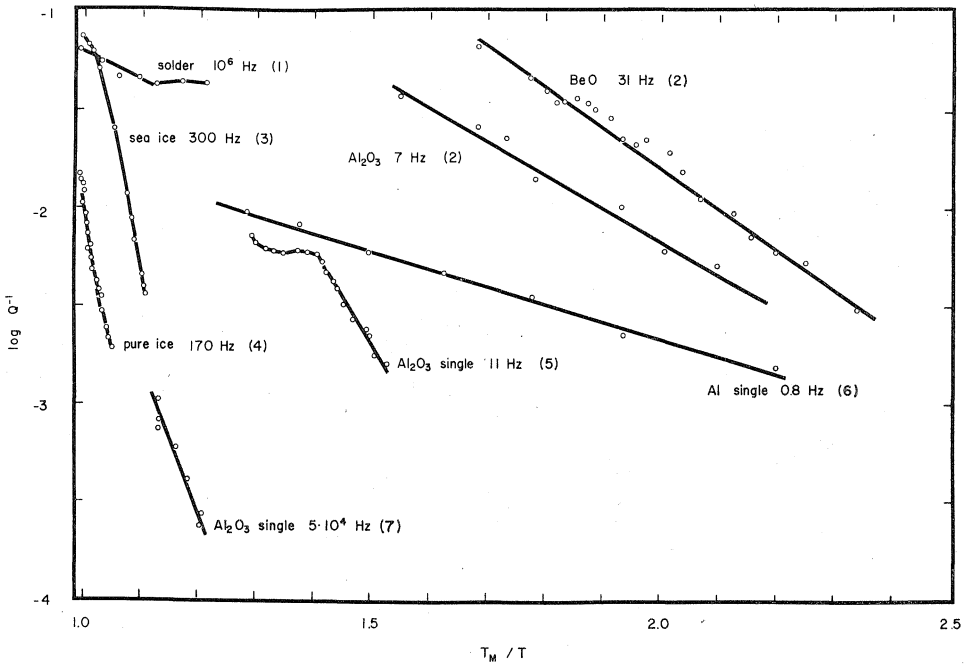

Fig. 19. High-temperature, internal-friction background for selected oxides and metals. Samples are polycrystalline unless otherwise noted. The Al_2O_3 single-crystal specimens were cold worked to introduce dislocations before testing. Data from: (1) *Mizutani and Kanamori* [1964]; (2) *Chang* [1959]; (3) *Tabata* [1959]; (4) *Kuroiwa* [1964]; (5) *Chang* [1961]; (6) *Kê* [1947]; (7) *Huber et al.* [1961]. Note that the effect of temperature on the attenuation in oxides is much greater than in the metals.

Studies of the melting of polycrystalline solids have shown that melting begins at grain boundaries, often at temperatures far below the melting point of the main constituents of the grains. This effect is caused by impurities that have collected at the grain boundaries during the initial solidification. *Walsh* [1968, 1969] computed the internal friction for two phenomenological models of a partially melted solid based on these observations. His calculations included mechanical effects only, ignoring thermoelastic and thermochemical attenuation in two-phase systems. In the first model, he assumed a structure of solid, perfectly elastic matrix with narrow lens-shaped inclusions of Newtonian viscous melt. For this model, if $\omega \ll \omega_c$, $c \ll 1$, and $Q^{-1} \ll 1$,

$$Q_K^{-1} = \frac{c(\omega/\omega_c)(K_1 - K_2)^2}{K_1(K_2 + cK_1)} \tag{19}$$

$$Q_\mu^{-1} = A\,\frac{\omega/\omega_d}{1 + A + \omega^2/\omega_d^2}$$

$$A = \frac{4}{15}(d^3/v)\left[\frac{1-\nu}{2-\nu}\right]$$

where Q_K^{-1} is internal friction for pure compression.

Q_μ^{-1} is internal friction for shear.
C is fractional concentration of melt phase.
K_s is bulk modulus of solid phase.
K_l is bulk modulus of melt phase.
d is major axis of melt inclusion.
v is average volume of solid material surrounding inclusion.
ν is Poisson ratio for solid material.
ω_c $= 3K_l/2\eta$.
ω_d $= a\mu_l/\eta$.
μ_l is shear modulus of melt phase.
μ_s is shear modulus of solid phase.
η is effective viscosity of melt in narrow channels.
a $= (3\pi\alpha/4)(3K_s + 2\mu_s)/(3K_s + 4\mu_s)$.
α is ratio of minor to major axes of the inclusion.

The restriction on ω is not at all severe, as $\omega_c > 10^8$ Hz for most liquids. The restrictions on c and Q^{-1} will hold almost up to the point of complete melting.

Attenuation according to Walsh's model should exhibit the following properties:

(*a*) Q_K^{-1}, the attenuation of the purely compressional component of seismic waves due to this mechanism, will be negligible at seismic frequencies, since $\omega_c \geq 10^8$ Hz for typical rocks.

(*b*) Under shear, this material exhibits the properties of the 'standard linear solid' with relaxation time roughly given by

$$1/\tau = \omega_d = a\mu_l/\eta$$

The ratio μ_l/η typically ranges from 10^4 to 10^8 Hz, so that this mechanism would be important for inclusion aspect ratios of 10^{-8} to 10^{-4}. These aspect ratios would be quite reasonable, assuming a melt phase that wets the grain boundary, thus forming a thin film. Furthermore, the relaxation strength A is strongly dependent on the number of sites of melting, and could exceed 1 even for a very small volume of melt.

(*c*) Assuming the viscosity behaves as $\eta = \eta_0 \exp(H^*/RT)$, this shear attenuation mechanism will behave as a thermally activated relaxation, comparable to the 'grain boundary viscosity' model of *Kê* [1949] (c.f. equation 9).

(*d*) Shear attenuation will increase very sharply with the onset of melting.

In the second model, the fluid phase is considered continuous, and the solid phase is described as spherical grains in the fluid matrix. Under the same restrictions on ω, c, and Q^{-1},

$$Q_K^{-1} = \frac{c(\omega/\omega_c)(K_S - K_l)^2}{K_S(K_l - cK_S)}$$
$$Q_\mu^{-1} = \frac{(8c/15)(\omega_c/\omega)(\mu/K_l)}{1 - (4c/15)(\mu/K_l)} \qquad (20)$$

The concentration of melt as a function of temperature and pressure is perhaps the most important unknown quantity in these equations, followed closely by the viscosity of the melt. As some partial melting is likely to occur in the earth's mantle, this mechanism is a possible cause of seismic attenuation, particularly at very low frequencies. Melt concentrations of as little as 10^{-5} may cause significant attenuation at seismic frequencies.

Spetzler and Anderson [1968] studied the effect of partial melting in the system NaCl-H_2O. At the eutectic temperature the system is partially molten, having a melt content that is proportional to the original salinity. The internal friction for longitudinal waves increased abruptly by 48% at the eutectic point for one per cent partial melting and 71% for two per cent partial melting. The corresponding increases in internal friction for shear were 37% and 73%. Further melting caused a gradual further increase in Q^{-1}. The fractional increases in Q^{-1} across the eutectic point were much greater than the fractional drops in velocity. Figure 20 shows the Q in the ice-brine-NaCl system for a concentration of 2% NaCl for longitudinal vibrations of a rod. Plotted are data for the fundamental and first two overtones. Note the abrupt drop in Q as partial melting is initiated at the eutectic temperature. There is a corresponding, but much less pronounced, drop in velocity at the same temperature.

SUMMARY

Several internal friction mechanisms can be ruled out almost immediately as significant causes of seismic attenuation in the earth's mantle. Rayleigh scattering, dislocation resonance, and bulk thermoelastic relaxation operate only at very high frequency. Magnetic relaxation will be unimportant in mantle materials. Friction across cracks, which probably causes most of the attenuation in dry rocks at low pressure, will not be important under mantle pressures.

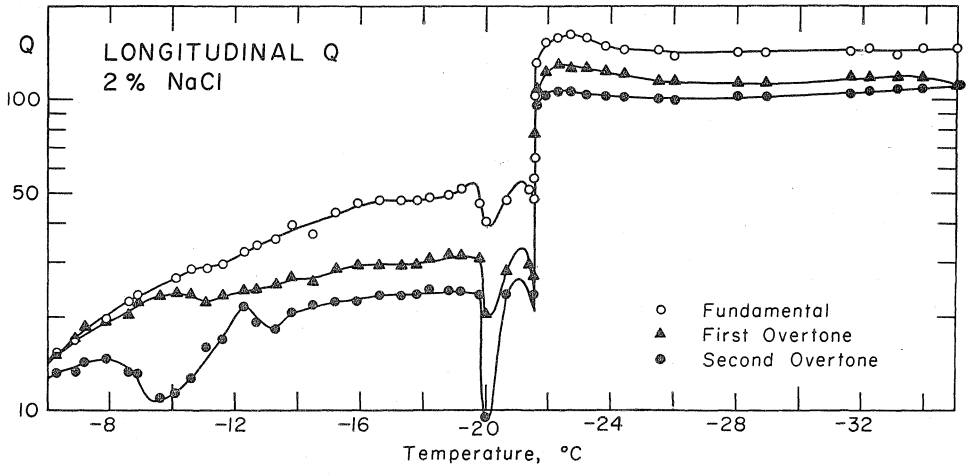

Fig. 20. Q measured from longitudinal vibrations of ice rod containing 2% NaCl. At low temperatures, this is a solid solution. At temperatures higher than the eutectic, the system is an ice-brine mixture.

A few mechanisms are unlikely to cause significant seismic attenuation in the upper mantle but cannot be ruled out completely. These include most of the high-frequency atomic scale relaxations, such as stress-induced ordering, twinning-detwinning, and stress-driven phase changes. Granato-Lücke dislocation hysteresis will probably not be important because of thermal unpinning of dislocations at high temperatures. Bordoni dislocation relaxation usually occurs only in deformed materials and at very low temperatures, and thus probably not in the earth's mantle, but recent experiments on aluminum oxide may have revealed a Bordoni peak at high temperatures.

Other mechanisms are likely to cause seismic attenuation, but their importance depends on factors that are very difficult to estimate. Intergranular thermoelastic relaxation depends on the grain size and thermal diffusivity of mantle materials. Relaxation caused by impurity diffusion, particularly at grain boundaries, is a very probable mechanism, but depends on details of the chemistry of the mantle, as well as grain size.

Grain-boundary relaxation and high-temperature background are the most probable mechanisms of seismic attenuation in the mantle, although partial melting may predominate in the low-velocity zone of the upper mantle.

Acknowledgments. The research was partly supported by the Air Force Office of Scientific Research, Office of Aerospace Research, United States Air Force, under AFOSR contract AF-49(638)-1337; National Science Foundation Grant GA 1003 (High Pressure); and the National Aeronautics and Space Administration under NASA Grant NGR 22-009-176.

REFERENCES

Alers, George A., Internal friction of quartz, *J. Appl. Phys., 24*(3), 103, 1964.

Alsop, L. E., G. H. Sutton, and M. Ewing, Measurement of *Q* for very long period free oscillations, *J. Geophys. Res., 66,* 2911, 1961.

Anderson, Don L., Universal dispersion tables, 1, Love waves across oceans and continents on a spherical earth, *Bull. Seismol. Soc. Amer. 54*(2), 681, 1964.

Anderson, Don L., The anelasticity of the mantle, *Geophys. J., 14,* 135, 1967.

Anderson, D. L., and C. B. Archambeau, The anelasticity of the earth, *J. Geophys. Res., 69*(10), 2071, 1964.

Anderson, Don L., A. Ben-Menahem, and C. B. Archambeau, Attenuation of seismic energy in the upper mantle, *J. Geophys. Res., 70*(6), 1441, 1965.

Anderson, Don L., and Robert L. Kovach, Attenuation in the mantle and rigidity of the core from multiply reflected core phases, *Proc. Nat. Acad. Sci. U.S., 51*(2), 168, 1964.

Anderson, Don L., and Charles Sammis, The low-velocity zone, *Proc. Pan-Amer. Conf. Upper Mantle Project,* Mexico D. F., Mexico, 1968, in press, 1969.

Asada, T., and K. Takano, Attenuation of short period *P* waves in the mantle, *J. Phys. Earth Tokyo, 11,* 25, 1963.

Bath, M., and A. Lopez-Arroyo, Attenuation and dispersion of *G* waves, *J. Geophys. Res., 67,* 1933, 1962.

Benioff, H., F. Press, and S. Smith, Excitation of the free oscillations of the earth by earthquakes, *J. Geophys. Res., 66,* 605, 1961.

Ben-Menahem, Ari, Observed attenuation and *Q* values of seismic waves in the upper mantle, *J. Geophys. Res., 70,* 4641, 1965.

Berry, B. S., Review of internal friction due to point defects, *Acta Met. 10,* 271, 1962.

Bhatia, A. B., *Ultrasonic Absorption,* Clarendon Press, Oxford, 1967.

Birch, Francis, and Dennison Bancroft, The effect of pressure on the rigidity of rocks, 1, *J. Geol., 46,* 59, 1938.

Bullard, E. C., The density within the earth, *Verhandel, Koninkl. Ned. Geol.-Mijn. Genoot., Geol. Ser., 18,* 23, 1957.

Carnahan, R. D., and J. O. Brittain, Point defect relaxation in rutile single crystals, *J. Appl. Phys., 34*(10), 3095, 1963.

Carnahan, R. D., and J. O. Brittain, Dislocation damping in rutile single crystals, *J. Amer. Ceram. Soc., 49*(1), 16, 1966.

Carpenter, E. W., Teleseismic methods for the detection, identification and location of underground explosions, *Rep. Inst. Sci. Tech.,* University of Michigan, 1964.

Chang, Roger, High temperature creep and anelastic phenomena in polycrystalline refractory oxides, *J. Nucl. Mater., 2,* 174, 1959.

Chang, Roger, Dislocation relaxation phenomena in oxide crystals, *J. Appl. Phys., 32*(6), 1127, 1961.

Chung, Dae-Hyun, Elastic and anelastic properties of fine-grained polycrystalline alumina at elevated temperatures, *Bull. Ceram. Res., 26*(297), 1961.

Chung, D., W. B. Crandall, and T. J. Gray, High temperature elastic and anelastic properties of alumina and alumina containing impurities, paper presented at Amer. Ceram. Soc. Meeting, New York, 1962.

Connes, J. P., A. Blum, G. Jobert, and N. Jobert, Observations des oscillations propres de la terre, *Ann. Geophys., 18,* 260, 1962.

Cook, Richard, and Robert G. Breckenridge, Anelasticity of quartz, *Phys. Rev., 92*(6), 1419, 1953.

Crandall, W. B., D. H. Chung, and T. J. Gray, The mechanical properties of ultra-fine hot pressed alumina, in *Mechanical Properties of Engineering Ceramics,* edited by W. Kriegel and H. Palmour, Interscience, New York, 1961.

Dahlberg, P., R. D. Carnahan, and J. O. Brittain, Dislocation damping in magnesium oxide crystals at low frequencies, *J. Appl. Phys., 33*(12), 3493, 1962.

Dew, Robert J., Damping capacity measurements on refractory oxides under varying stress and temperature conditions, ScD. thesis, Dept. of Metallurgy, M.I.T., Cambridge, Mass., 1950.

Donth, Hans, Zur Theorie des Tieftemperaturmaximums der inneren Reibung von Metallen, *Z. Phys., 149,* 111, 1957.

Dorman, L. M., Anelasticity and the spectra of body waves, *J. Geophys. Res., 73*(12), 3877, 1968.

Ewing, M., and F. Press, An investigation of mantle Rayleigh waves, *Bull. Seismol. Soc. Amer., 44,* 127, 1954*a*.

Ewing, M., and F. Press, Mantle Rayleigh waves from Kamchatka earthquake, *Bull. Seismol. Soc. Amer., 44,* 471, 1954*b*.

Fedotov, S. A., Absorption of transverse seismic waves in the upper mantle and energy classification of near earthquakes of intermediate focal depths, *Izv. Akad. Nauk SSSR, Ser. Geofiz., 1963,* 509, 1963.

Fitzgerald, J. V., Anelasticity of glass, 1, *J. Amer. Ceram. Soc., 34*(10), 314, 1951.

Forry, K. E., Two peaks in the internal friction as a function of temperature in some soda silicate glasses, *J. Amer. Ceram. Soc., 40*(3), 90, 1957.

Fraser, David B., Anelastic effects of alkali ions in crystalline quartz, *J. Appl. Phys., 35*(10), 2913, 1964.

Futterman, W. I., Dispersive body waves, *J. Geophys. Res., 67*(13), 5257, 1962.

Gellings, P. J., Measures used in describing the damping of ultrasound, *Acoustica, 11,* 363, 1961.

Gordon, R. B., and Carl Nelson, Anelastic properties of the earth, *Rev. Geophys., 4*(4), 457, 1966.

Granato, A., and K. Lücke, Theory of mechanical damping due to dislocations, *J. Appl. Phys., 27*(6), 583, 1956.

Gutenberg, B., Dispersion und Extinktion von seismischen Oberflachenwellen und der aufban der obersten Erdschichten, *Z. Phys., 25,* 377, 1924.

Gutenberg, B., Amplitudes of *P, PP,* and *S* and magnitude of shallow earthquakes, *Bull. Seismol. Soc. Amer., 35,* 57, 1945.

Gutenberg, B., Attenuation of seismic waves in the earth's mantle, *Bull. Seismol. Soc. Amer., 48,* 269–282, 1958.

Hiki, Yosio, Internal friction of quartz, *J. Phys. Soc. Japan, 15*(4), 586, 1960.

Hiki, Yosio, Internal friction of synthetic quartz, *J. Phys. Soc. Japan, 16*(4), 664, 1961.

Hirasawa, T., and K. Takano, Differential attenuation of *P* waves as derived from a Hindu-Kush earthquake, *J. Phys. Earth Tokyo, 14,* 49, 1966.

Huber, R. J., G. S. Baker, and P. Gibbs, High temperature kilocycle internal friction in Al_2O_3 single crystals, *J. Appl. Phys., 32*(12), 2573, 1961.

Jackson, D. D., Elastic relaxation model for seismic wave attenuation in the earth, *Phys. Earth Planet. Interiors, 2,* 30, 1969.

Kamentsky, L. A., A study of the internal friction and Young's modulus of pure copper single crystals in the temperature range 25°C to 750°C, Ph.D. thesis, Cornell University, Ithaca, New York, 1957.

Kanamori, H., Spectrum of *P* and *PcP* in relation to the mantle-core boundary and attenuation in the mantle, *J. Geophys. Res., 72,* 559, 1967*a*.

Kanamori, H., Spectrum of short-period core phases in relation to the attenuation in the mantle, *J. Geophys. Res., 72,* 2181, 1967*b*.

Kanamori, Hiroo, Attenuation of *P* waves in the upper and lower mantle, *Bull. Earthquake Res. Inst. Tokyo Univ., 45,* 299, 1967*c*.

Kê, T. S., Experimental evidence of the viscous behavior of grain boundary in metals, *Phys. Rev., 71*(8), 533, 1947.

Kê, T'ing-Sui, A grain boundary model and the mechanism of viscous intercrystalline slip, *J. Appl. Phys., 20*(3), 274, 1949.

Khorosheva, V. V., Some results of the investigation of *Pa* and *Sa* waves from the seismograms of the USSR, *Izv. Akad. Nauk SSSR, Ser. Geophys., 1960*(11), 1960.

Knopoff, Leon, *Q, Rev. Geophys., 2*(4), 625, 1964.

Knopoff, L., and G. J. F. MacDonald, Models for acoustic loss in solids, *J. Geophys. Res., 65*(7), 2191, 1960.

Kovach, Robert L., and Don L. Anderson, Attenuation of shear waves in the upper and lower mantle, *J. Geophys. Res., 54*(6), 1855, 1964.

Kuroiwa, Daisuke, Internal friction of ice, *Contrib. Inst. Low Temp. Sci.,* Hokkaido Univ., Sapporo, Japan, 1964.

Leak, G. M., Grain boundaries and surface properties of metals, *Progr. Appl. Mater. Res., 4,* 1, 1962.

MacDonald, Gordon J. F., Calculations on the thermal history of the earth, *J. Geophys. Res., 64*(11), 1967, 1959.

MacDonald, G. J. F., and N. F. Ness, A study of the free oscillations of the earth, *J. Geophys. Res., 66,* 1865, 1961.

McGinley, J., and D. L. Anderson, Relative amplitudes of *P* and *S* waves as a mantle reconnaissance tool, *Bull. Seismol. Soc. Amer., 59*(3), 1189, 1969.

Marx, J. W., and J. M. Sivertsen, Temperature dependence of the elastic moduli and internal friction of silica and glass, *J. Appl. Phys., 24*(1), 81, 1953.

Mason, Warren P., *Physical Acoustics and the Properties of Solids,* D. Van Nostrand, Princeton, N. J., 1958.

Mizutani, H., and H. Kanamori, Variation of elastic wave and attenuative property near the melting point, *J. Phys. Earth Tokyo, 12*(2), 43, 1964.

Mohyuddin, Iftikhar, and R. W. Douglas, Some observations of the anelasticity of glasses, *Phys. Chem. Glasses, 1*(3), 71, 1960, and correction *4*(1), 34, 1963.

Mott, N. F., Slip at grain boundaries and grain growth in metals, *Proc. Phys. Soc., 60,* 391, 1948.

Nachtrieb, N. H., J. Petit, and J. Wehrenberg, Self diffusion of silver in silver-palladium alloys, *J. Chem. Phys., 26,* 106, 1957.

Ness, N. F., J. C. Harrison, and L. B. Slichter, Observations of the free oscillations of the earth, *J. Geophys. Res., 66,* 621, 1961.

Niblett, D. H., and J. Wilks, Dislocation damping in metals, *Advan. Phys., 9*(33), 1, 1960.

Nowroozi, A. A., Measurement of Q values from the free oscillations of the earth, *J. Geophys. Res., 73*(4), 1407, 1968.

O'Brien, P. N. S., Lake Superior crustal structure—A reinterpretation of the 1963 seismic experiment, *J. Geophys. Res., 73*(8), 2669, 1968.

Otsuka, M., On the forms of the *S* and *ScS* waves of some deep earthquakes (in Japanese), *Zisin,* [*2*]*15*(3), 169, 1962.

Otsuka, M., Some considerations on the wave forms of *ScS* phases, *Spec. Contrib. Geophys. Inst., Kyoto University, No. 2,* 415, 1963.

Pearson, S., and L. Rotherham, Internal friction and grain boundary viscosity of silver and binary silver solid solutions, *J. Metals, 8,* 894, 1956.

Popov, I. I., Dispersion of long period Love waves in the continental and oceanic crust along the path Indonesia-Crimea, *Izv. Akad. Nauk USSR, Ser. Geophys., 1960*(10), 1960.

Press, Frank, Rigidity of the earth's core, *Science, 124*(3233), 1204, 1956.

Press, Frank, A. Ben-Menahem, and M. N. Toksoz, Experimental determination of earthquake fault length and rupture velocity, *J. Geophys. Res., 66,* 3471, 1961.

Press, Frank, Seismic wave attenuation in the crust, *J. Geophys. Res., 69*(20), 4417, 1964.

Randall, R. H., F. C. Rose, and C. Zener, Intercrystalline thermal currents as a source of internal friction, *Phys. Rev., 56,* 343, 1939.

Read, T. A., Internal friction of single metal crystals, *Phys. Rev., 58,* 371, 1940.

Sato, R., and A. F. Espinosa, Dissipation in the earth's mantle and rigidity and viscosity in the earth's core determined from waves multiply reflected from the mantle-core boundary, *Trans. Amer. Geophys. Union, 46*(1), 158, 1965.

Sato, R., and A. F. Espinosa, Dissipation in the earth's mantle and rigidity and viscosity in the earth's core determined from waves multiply reflected from the mantle-core boundary, *Bull. Seismol. Soc. Amer., 57,* 829, 1967.

Satô, Y., Attenuation, dispersion, and the wave guide of the *G* wave, *Bull. Seismol. Soc. Amer., 48,* 231, 1958.

Savage, J. C., Thermoelastic attenuation of elastic waves by cracks, *J. Geophys. Res., 71*(16), 3929, 1966.

Savage, J. C., Thermoelastic attenuation of elastic waves in the mantle, paper presented at 48th Annual Meeting, American Geophysical Union, Washington, D. C., 1967.

Savarensky, E. F., I. I. Popov, and A. P. Lazareva, Observations of long period waves of the Chilean earthquake of 1960, *Izv. Akad. Nauk SSSR, Ser. Geophys., 1961,* 774, 1961.

Savarensky, E. F., I. L. Nersesov, R. M. Karmaleeva, and L. A. Latynina, Long-period waves of the Aleutian earthquake of 4 February, 1965, recorded by quartz extensometers, *Izv. Earth Phys. 1966*(5), 33, 1966.

Slichter, L. B., Spherical oscillations of the earth, *Geophys. J., 14*(1–4), 171, 1967.

Smith, S. W., An investigation of the earth's free oscillations, Ph.D. thesis, California Institute of Technology, Pasadena, 1961.

Snoek, J. L., Effect of small quantities of carbon and nitrogen on the elastic and plastic properties of iron, *Physica, 8,* 711, 1941.

Southgate, P. D., Mechanical relaxation of a point defect in magnesium oxide, *J. Appl. Phys., 36*(9), 2696, 1965.

Southgate, P. D., Internal friction due to chromium and iron in magnesium oxide, *J. Phys. Chem. Solids, 27,* 1263, 1966.

Southgate, P. D., K. S. Mendelson, and P. L. DePerro, Kilocycle-range dislocation damping in MgO, *J. Appl. Phys., 37*(1), 206, 1966.

Spetzler, H., and D. L. Anderson, The effect of temperature and partial melting on velocity and attenuation in a simple binary system, *J. Geophys. Res., 73*(18), 6051, 1968.

Steinhart, J. S., Suzuki, T. J. Smith, L. T. Aldrich, and I. S. Sacks, Explosion seismology, *Carnegie Inst. Wash. Yr. Book 63,* 311, 1964.

Strakna, R. E., and H. T. Savage, Ultrasonic relaxation loss in SiO_2, GeO_2, B_2O_3, and As_2O_3 glass, *J. Appl. Phys., 35*(5), 1445, 1964.

Strick, E., The determination of *Q*, dynamic viscosity and transient creep curves from wave propagation measurements, *Geophys. J., 13*, 197, 1967.

Tabata, Tadashi, Studies on mechanical properties of sea ice, 4, Measurement of internal friction, *Low Temp. Sci., Ser. A, 18*, 131, 1959.

Teng, T. L., Body wave and earthquake source studies, chapter 7 in Attenuation of Body Waves and the *Q* Structure of the Mantle, Ph.D. thesis, California Institute of Technology, Pasadena, 1966.

Turnbaugh, J. E., Effects of additions on the high-temperature grain-boundary relaxations of alumina, Sc.D. thesis, Dept. of Metallurgy, M.I.T., Cambridge, Mass., 1962.

Turnbaugh, J. E., and F. H. Norton, Low-frequency grain-boundary relaxation in alumina, *J. Amer. Ceram. Soc., 51*(6), 344, 1968.

Ubbelohde, A. R., *Melting and Crystal Structure,* Clarendon Press, Oxford, 1965.

Utsu, T., Regional differences in absorption of seismic waves in the upper mantle as inferred from abnormal distributions of seismic intensities, *J. Fac. Sci., Hokkaido Univ.,* [*8*]*2*, 359, 1966.

Vaišnys, J. R., Propagation of acoustic waves through a system undergoing phase transformations, *J. Geophys. Res., 73*(24), 7675, 1968.

Van Bueren, H. G., *Imperfections in Crystals,* North-Holland Publishing Company, Amsterdam, 1961.

Volarovich, M. P., and A. S. Gurvitch, Investigation of dynamic moduli of elasticity for rocks in relation to temperature, *Bull. Acad. Sci. USSR, Geophys. Ser., 1957*(4), 1, 1957.

Wachtman, J. B., Mechanical and electrical relaxation in ThO_2 containing CaO, *Phys. Rev., 131*(2), 517, 1963.

Wachtman, J. B., and W. C. Corwin, Internal friction in ZrO_2 containing CaO, *J. Res. NBS, 69A*(5), 457, 1965.

Wachtman, J. B., and D. G. Lam, Factors controlling resistance to deformation and mechanical failure in polycrystalline (glass-free) ceramics, *NBS. Rep. 5770* (Progr. Rep. 27), 1958.

Wachtman, J. B., and L. H. Maxwell, Plastic deformation of ceramic oxide single crystals, 2, *J. Amer. Ceram. Soc., 40*(11), 377, 1957.

Wachtman, J. B., H. S. Peiser, and E. P. Levine, Symmetry splitting of equivalent sites in oxide crystals and related mechanical effects, *J. Res. NBS, 67A*(4), 281, 1963.

Wachtman, J. B., W. E. Tefft, D. G. Lam, and R. P. Stinchfield, Factors controlling resistance to deformation and mechanical failure in polycrystalline (glass-free) ceramics, *WADC-Tech. Rep. 59-278,* 1959.

Wadati, K., and T. Hirono, Magnitude of earthquakes—especially of near, deep focus earthquakes, *Geophys. Mag., 27*(1), 1, 1956.

Walsh, J. B., Seismic wave attenuation in rock due to friction, *J. Geophys. Res., 71*(10), 2591, 1966.

Walsh, J. B., Attenuation in partially melted material, *J. Geophys. Res., 73*(6), 2209, 1968.

Walsh, J. B., A new analysis of attenuation in partially melted rock, *J. Geophys. Res., 74*, 4333, 1969.

Wilson, J. T., The Love waves of the South Atlantic earthquake of August 28, 1933, *Bull. Seismol. Soc. Amer., 30*, 273, 1940.

Wasilik, John H., Anisotropic relaxation peak in the internal friction of crystalline quartz, *Phys. Rev., 105*(4), 1174, 1957.

Whitelaw, J. H., An experimental investigation of the internal friction of small diameter quartz strands at low frequencies, *J. Sci. Instrum., 41*(4), 215, 1964.

Zener, Clarence, *Elasticity and Anelasticity of Metals,* University of Chicago Press, Chicago, Illinois, 1948.

Zener, Clarence, and R. H. Randall, Variation of internal friction with grain size, *Trans. AIME, 137*, 41, 1940.

(Manuscript received July 1968; revised May 3, 1969.)